Master Thesis

Prediction of Diesel Oxidation Catalyst Aging

KE202X Degree Project in Chemical Engineering, Second Cycle, 30 hp

KTH – Royal Institute of Technology

Author:
Filip Gruvnäs

Supervisor:
David Raymand, Ph. D.

Examiner:
Prof. Lars Pettersson

August 24, 2015

Abstract

A conventional exhaust gas after treatment system (EATS) for the Euro VI legislation contains four different catalyst. The first two (particulate filter system) remove particulates and the last two (SCR system) remove nitrogen oxides (NO_x). The particulate filter system also optimizes the gas composition with respect to nitrogen monoxide (NO) and nitrogen dioxide (NO_2). The performance of the SCR system has a strong dependency on the NO:NO_2 ratio as the so called selective catalytic reduction (SCR) reaction is kinetically favored at a NO:NO_2 ratio of 1:1.

The diesel oxidation catalyst (DOC) is placed first in the EATS. Due to this placement, the DOC is subjected to a rough environment, e.g. high temperatures and oil/fuel impurities that with time will affect its performance, i.e. the catalyst ages.

In this master thesis, the aging of the DOC has been empirically correlated to thermal load and sulfur exposure. The study shows that it is possible to predict how the NO oxidation performance decays as a function of thermal and sulfur exposure. The empirical relation was fitted against two aging cycles and validated against an additional four. The results show that the loss of catalytic activity can to a large extent be explained by the cycle it has been used on.

Sammandrag

Ett konventionellt efterbehandlingssystem för Euro VI-standarden innehåller fyra olika katalysatorer. De första två rensar (partikelfiltersystemet) från partiklar och de två sista (SCR-systemet) tar bort kväveoxider (NO_x). Partikelfiltersystemet reglerar även gassammansättningen med avseende på kvävemonoxid (NO) och kvävedioxid (NO_2). Prestandan för SCR-systemet har ett starkt beroende på NO:NO_2-förhållandet där ett förhållande på 1:1 är kinetiskt gynnat för den så kallade SCR-reaktionen (*eng:* Selective Catalytic Reduction).

Oxidationskatalysatorn (DOC) sitter som ett första steg i efterbehandlingen. Placeringen medför att katalysatorn finns i en tuff miljö där den till exempel utsätts för hög temperatur och olje/bränsle-föroreningar som över tiden påverkar dess prestanda. Detta brukar kallas att DOC:n åldras.

I detta examensarbete har åldrandet av DOC:n korrelerats empiriskt till termisk belastning och svavel-exponering. Studien visar att det är möjligt att förutsäga hur NO-oxidationsprestandan avtar som en funktion av termisk last och svavelexponering. Det empiriska modellen anpassades till två åldringscykler och validerades emot ytterligare fyra cykler. Resultaten visar att den kvarvarande katalytiska aktiviteten i stor utsträckning kan förklaras genom vilken cykel den har körts på.

Acknowledgments

This master thesis was performed during the spring of 2015 at Scania CV AB, Research & Development, group NMTK (catalytic converter and particulate filter performance). I would like to thank the group and department for a good work environment where I really enjoyed working. This report has been audited and allowed publication. Sensitive information has been excluded.

I would like to start thanking my examiner, Lars Pettersson, for his interesting lectures at KTH which I always enjoyed and got me interested in catalysis. Next, I would like to thank Henrik Grimler for being able to answer my every LaTeX related question. I would also like to thank my girlfriend, Fannie Sillén, for support and putting up with all the stress during my five years of study.

I end with special thanks to my supervisor, David Raymand, for taking time to discuss the problems that arose during the thesis, for endless re-reading of my report and for always being encouraging. Thanks a lot!

Stockholm, June 2015

Filip Gruvnäs

Contents

List of Figures

List of Tables

Chapter 1

Background

1.1 Introduction

Transport and logistic companies depend on heavy duty vehicles, ranging from waste collection in urban environments to long-haulage freight trucking. Most of these vehicles are propelled by a diesel engine. The diesel engine has several advantages in comparison to the gasoline engine, such as higher efficiency, longer lifetime and a lean combustion leading to lower gaseous NO_x, CO and Hydrocarbon (HC) emissions [1].

The main constituents of the diesel exhaust gas are CO_2 (2–12 %), H_2O (2–12 %), O_2 (3–17 %) and N_2 (balance) [2]. All these substances are regarded as non-hazardous. However, during combustion, unwanted byproducts are also formed. These include incompletely oxidized substances (HC and CO), Particulate Matter (PM), NO_x and other substances such as SO_x. One of the main components of concern and interest in the diesel exhaust is NO_x, which is a source of acid rain, smog formation and ozone depletion. NO_x from diesel engines primarily originates from the N_2 and O_2 in the air, defined as thermal NO_x.

The first real measure to regulate emissions from heavy duty diesel engines in Europe was introduced in 1992 with the implementation of the Euro I emission legislation. Euro I had limits for CO, HC, NO_x and PM. Since then, the emission limits have become successively more stringent with new emission standards for heavy duty vehicles to further suppress the environmental impingement. The latest European emission standard is Euro VI, in effect since 2013, which adds a regulation for the Particulate Number (PN). The emission limits for the World Harmonized Stationary Cycle (WHSC) and the World Harmonized Transient Cycle (WHTC) for Euro VI are summarized in *Table* 1.1. Apart from the emission limits the fuel quality is also regulated with respect to sulfur content which can have a large negative impact on treatment of the exhaust gas to meet the limits. In 1994, the sulfur limit for diesel was 2000 ppm and today it is regulated as a maximum of 10 ppm.

Table 1.1: Emission standard for Euro VI

Cycle	CO [mg/kWh]	HC [mg/kWh]	NO_x [mg/kWh]	NH_3 [ppm]	PM [mg/kWh]	PN [#/kWh]
WHSC	1500	130	400	10	10	8.0×10^{11}
WHTC	4000	160	460	10	10	6.0×10^{11}

To meet the emission limits, heavy duty vehicle manufacturers have to use a mix of engine measures and exhaust gas treatment, with a trend towards developing the latter. The techniques for the exhaust treatment differ among manufacturers, but what is standard is the usage of catalysts.

1.2 Exhaust Catalysis

The Exhaust gas After Treatment System (EATS) is dependent on catalysis, or more specifically heterogeneous catalysis, which is defined as the catalyst and reactants being in different phases (e.g. a NO and O_2 molecule reacting on a monolith surface to produce NO_2). Catalysis does not affect the thermodynamics, but the kinetics are improved by altering the reaction path. The reactions that take place in the EATS are slow at prevailing temperatures and catalysis is therefore a necessity. Generally, when referring to a catalyst it includes a substrate, a washcoat and active material. Taking the Diesel Oxidation Catalyst (DOC) as an example, it most often comprises of a cordierite monolith substrate, an Al_2O_3 washcoat and active material Pt/Pd.

The washcoat is an aid to increase the specific surface area of the catalyst. Important properties of the washcoat include high specific surface area, thermal resistance and inertness. Using a high surface area washcoat increases the dispersion of the precious metals, therefore increasing the activity of the catalyst. Dispersion is defined as number of surface atoms divided by the total number of atoms [11].

The active materials are the active sites for reaction that are responsible for the increase in kinetics. The washcoat can also act as active material, thus serving two purposes.

Heterogeneous catalysis is very complex and therefore hard to model. The complexity originates from the heterogeneity (the two phases have to come in contact and then be separated). The steps in between can be identified as *external mass transfer* (bulk diffusion), *internal mass transfer* (pore diffusion in washcoat) and *surface adsorption/desorption/reaction*. Because of the complexity, theoretical models for heterogeneous catalysis are rare and empirical models are more common.

1.3 Exhaust Gas Treatment System in Scania Euro VI

To meet Euro VI, Scania has developed an EATS consisting of four different types of catalysts. The two first (particulate filter system) are responsible for oxidation reactions and particulate removal, and the last two (SCR-system) removes the NO_x. The performance of the EATS depends on the system as a whole, i.e. how the different catalysts interact and it cannot be reduced to individual catalyst activity. The catalyst that influences the other parts of the EATS the most is the DOC which is placed as a first step in the silencer. The downstream catalysts are heavily reliant on the DOC's performance and therefore its working principles have to be studied. This includes the factors that might influence its catalytic activity in a bid to optimize the EATS. The EATS of Scania's Euro VI can roughly be represented as five parts contained in a silencer:

i) Diesel Oxidation Catalyst (DOC)

ii) Diesel Particulate Filter (DPF)

iii) Urea Dosing System (UDS) and evaporation unit

iv) Selective Catalytic Reduction (SCR) catalyst

v) Ammonia Slip Catalyst (ASC)

The different parts will briefly be explained in the following sections. Through *Sections* 1.3.2 to 1.3.3, the working principle of the catalysts will be explained and in *Section* 1.3.4 the integration and dependency of different parts will be reviewed. A schematic overview of the silencer can be seen in *Figure* 1.1.

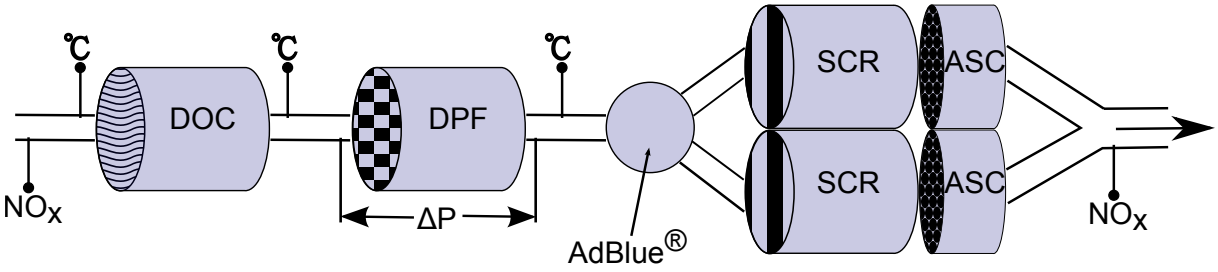

Figure 1.1: Schematic depiction of the EATS for Euro VI.

1.3.1 Diesel Oxidation Catalyst

The DOC is the first step in the cleaning of the exhaust gas. The reason for this placement is that its actions can aid the downstream processes to perform more optimal. The main purpose of the DOC is to oxidize CO and unburnt hydrocarbons (HC) to CO_2 and H_2O. In addition, it oxidizes NO to NO_2 which is utilized for different purposes (explained in *Section* 1.3.4). As stated, a typical DOC comprises of a cordierite monolith, Al_2O_3 washcoat and active catalytic precious metals Pt and Pd.

The DOC can be monometallic, but is preferably prepared as an alloy of precious metals to obtain desired properties. The most common alloy is bimetallic Pt and Pd, with the main advantage of being more resistant to sintering at higher temperatures than monometallic Pt DOCs [3]. However, research is made on monometallic Pt/TiO_2 catalysts as Pt and TiO_2 are much more sulfur resistant at low temperatures [4]. Despite Pt being more expensive and more sensitive to thermal degradation its presence is indispensable due to its excellent NO oxidation properties with low light-off temperature [5].

1.3.2 Diesel Particulate Filter

The DPF removes PM from the exhaust gas and is essential to meet the maximum PN allowed in the exhaust gas which is regulated from Euro VI. The DPF can be described as a porous ceramic monolith with alternating plugged channels at the inlet and outlet. This forces the exhaust gas to move through the ceramic wall and PM to be captured. This causes a pressure drop over the DPF which is proportional to the amount of soot and ash accumulated. The soot is continuously burnt off with NO_2 (passive regeneration) and due to the increase in kinetics at elevated temperatures, active measures are also possible (HC injection).

The DPF is basically comprised by the same substances as the DOC and hence can serve the same purpose. However, the precious metal loading is typically far less and the DPF will experience less oxidation activity per unit volume than the DOC.

1.3.3 SCR system

SCR catalyst (hereafter the catalyst is referred to as only SCR) is often used as a synonym for a catalyst reducing NO_x to N_2 and H_2O. The reduction can be performed through different approaches, e.g. HC-SCR and NH_3-SCR, where the latter is used in Scania's vehicles. The reducing agent used is NH_3 and the reaction is catalyzed with V_2O_5 with added WO_3 and TiO_2 as washcoat. The WO_3 is added to increase thermal stability and TiO_2 increases surface area in addition to having high resistance to sulfur poisoning [1]. AdBlue® (32.5 wt-% urea in H_2O) is supplied by the UDS and the urea decomposes to NH_3 which is mixed with the exhaust gas and reacts with the NO_x in the SCR. NO_x consists primarily of NO and NO_2 and the reducing reactions are the following:

$$4\,NH_3 + 4\,NO + O_2 \longrightarrow 4\,N_2 + 6\,H_2O \qquad \textit{(Normal SCR)} \qquad \text{(R 1.1)}$$

$$2\,NH_3 + NO + NO_2 \longrightarrow 2\,N_2 + 3\,H_2O \qquad \textit{(Fast SCR)} \qquad \text{(R 1.2)}$$

$$8\,NH_3 + 6\,NO_2 \longrightarrow 7\,N_2 + 12\,H_2O \qquad \textit{(Slow SCR)} \qquad \text{(R 1.3)}$$

where the desirable is *Reaction* (R 1.2) for kinetic reasons with a molar ratio of 1:1 between NO_2 and NO. When the exhaust gas is coming out from the engine the NO amount is much greater than the NO_2 amount. This can however be optimized through DOC design, which will be discussed in *Section* 1.3.4. Although optimal ratio is 1:1, it is more advantageous to be beneath 50 % NO_2 than above, due to having more NO_2 than NO favors *Reaction* (R 1.3) which is even slower than *Reaction* (R 1.1), and this is especially important for the V_2O_5 catalyst. Another thing to note is that the NH_3 to NO_x ratio (ANR) is 1:1 in *Reaction* (R 1.1) and (R 1.2) but increases to 4:3 for *Reaction* (R 1.3). After the SCR there is an additional catalyst, ASC, which is responsible to oxidize unreacted NH_3 that slips through the SCR.

1.3.4 Catalyst Integration and Dependency

As stated, the EATS is an integrated system where different catalysts' performance can heavily affect the performance of others. Discussed in *Section* 1.3.3, the optimal NO_2 to NO ratio is 1:1. When the

exhaust gas leaves the engine, the NO_x content is primarily NO (90–95 % [6], depends on e.g. driving conditions) and without any action, the performance of the SCR would not be optimized. In addition, the DPF needs NO_2 for kinetically favored oxidation of soot. Owing to these two reasons the best placement for the DOC is first in the EATS. The DPF also possesses oxidation properties and increases the NO_2 concentration further.

The DOC is tailored specifically for a vehicle in question with the right volume and precious metal loading in order to adjust the NO_2 to NO ratio. This implies that for a degreened DOC, the activity is enough to both oxidize HC and CO and also to oxidize the right amount of NO. When the DOC is being used, it ages and hence its NO oxidation performance decreases which directly affects the DPF, but most important the SCR.

1.3.4.1 Urea Dosing

Scania utilizes NH_3-SCR, where NH_3 is generated through urea decomposition. The urea dosing is critical, as over-dosing can induce an undesired NH_3-slip to the atmosphere. Over-dosing does not only cause extra cost, but it can also exceed the allowed emission limit if the ASC cannot manage the slip. Under-dosing of urea is of equal importance as it may cause insufficient reduction of NO_x and therefore not meet the NO_x emissions limit.

The urea dosing is based on feedback from NO_x sensors. In the silencer, there exist two NO_x sensors as depicted in *Figure* 1.1. The sensor upstream of the DOC determines the amount of urea to be injected from the UDS. The downstream sensor from the SCR-system is mandatory by law, used for both diagnosis and control. The NO_x sensors available today has different sensitivity for different NO_x and does also lack selectivity. The NO_x sensor does also register NH_3 as NO_x and its sensitivity decreases as $NO > NH_3 > NO_2$ [7]. As an example, 100 ppm NO gives the same signal as 80 ppm NO_2. If 100 % NO_2 is presumed, but it is in fact 100 % NO, the Electric Control Unit (ECU) overestimates the total NO_x concentration indicated by the NO_x sensors. Today there is only one commercially sold NO_x sensor manufactured in a cooperation between NGK (ceramic sensing element) and Continental (electronic control unit) and its performance is limited [7, 8].

The problem with differing sensitivity is compensated by the ECU, in a bid to increase the accuracy of the UDS. However, the compensation to control the UDS is calibrated for a "fresh" catalyst and after aging of the catalyst, the NO oxidation activity is significantly decreased. This implies that the NO_2 is overestimated by the ECU.

Another aspect worth mentioning is that the ANR is different, depending on the prevailing NO_2 to NO ratio. On page 3, the different reactions over the SCR catalyst are presented. The ANR is different for *Reaction* (R 1.3), compared to *Reactions* (R 1.1) and (R 1.2). At driving conditions yielding a composition higher than 50 % NO_2 post DPF, the stoichiometry for the SCR reaction might be wrong due to aging of the DOC. This is not limited to an increase in AdBlue® consumption, but also an increase in NH_3-slip that might be too much for the ASC to handle. This can lead to a non-selective NO_x sensor signal increase and therefore further errors.

If the aging can be correlated to factors influenced by the driving conditions for a specific vehicle, the ECU could adjust the urea dosing to the right amount.

1.4 Deactivation

One major concern for the DOC is deactivation which is a phenomenon that is common for all types of catalysts. The factors that may contribute to the deactivation of a catalyst can be seen in *Table* 1.2. The NO_2 net gain is also indirectly affected by decreasing activity for other reactions. As light-off temperatures for reductants (CO and HC) shifts to higher temperatures the excess reductants work to reduce NO_2 to NO [9].

As discussed, the DOC activity affects the whole EATS, especially the SCR. The NO oxidation over the DOC can be visualized with light-off curves. *Figure* 1.2 is specific for a DOC that has been run on a test bench engine for 2000 h. It is evident that with time the NO oxidation activity drops substantially

and the SCR performance will therefore be affected. Concerns regarding to this will be discussed in *Section* 1.5.

The deactivation can be divided into thermal and chemical deactivation which will be reviewed through *Sections* 1.4.1 and 1.4.2.

Table 1.2: How deactivation mechanisms affect the rate of a catalyzed reaction and the rapidity and reversibility of deactivation process [10]

	Effects on reaction rate		Deactivation process		
Deactivation mechanism	Decrease in number of active sites	Decrease in intrinsic activity	Decrease in effectiveness factor	Fast or slow[a]	Reversible
Chemical degradation	✓	✓	✓[b,c]	varies	no
Fouling	✓		✓	fast	yes
Mechanical degradation	✓		✓	varies	no
Sintering	✓	✓[b,d]	✓[b,e]	slow	sometimes
Vaporization/ Leaching	✓		✓[b,f]	fast	sometimes

[a] Generally.
[b] In some cases.
[c] Chemical degradation can cause breakdown of support, pore plugging, and loss of porosity.
[d] If the reaction is structure-sensitive, sintering could either increase or decrease intrinsic activity.
[e] Sintering of the support may cause support collapse and loss of porosity and it may also increase average pore diameter.
[f] Leaching of aluminum or other cations from zeolites can cause buildup of aluminum or other oxides in zeolite pores.

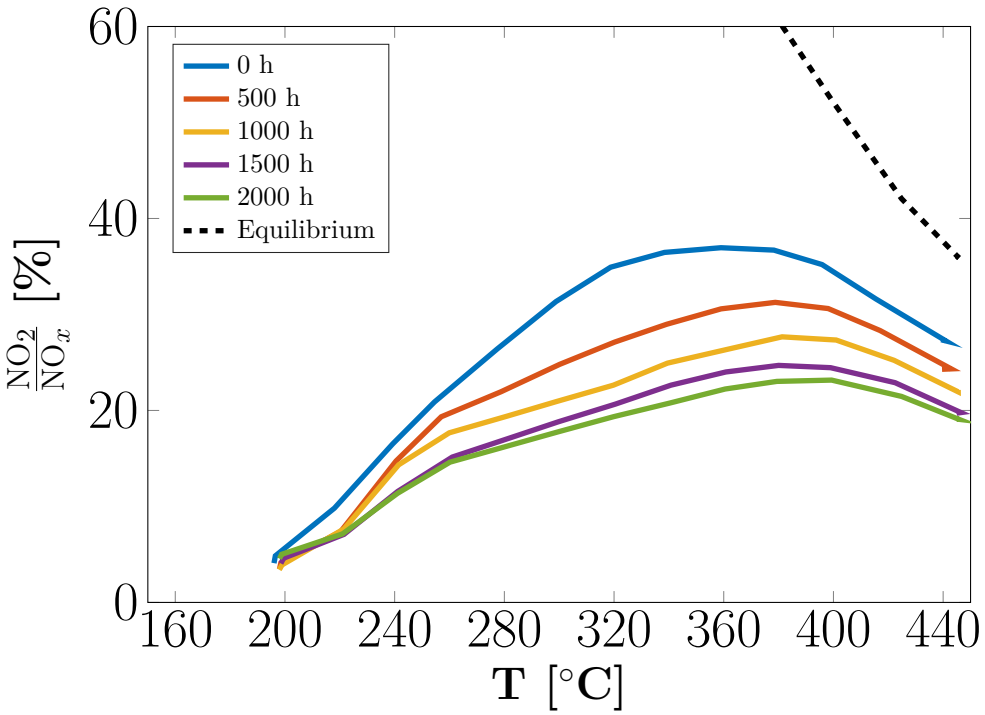

Figure 1.2: NO oxidation for DOC and how it changes over time.

1.4.1 Thermal Deactivation

Thermal deactivation, or sintering, is characterized by structural changes in the active surface area of the catalyst. When the washcoat is subjected to high temperatures it may undergo undesired phase transformation which lowers the specific surface area. Sintering acts to lower the surface energy of the washcoat through eliminating pores in the structure [3]. Thermal deactivation is less of a concern in the DOC than in the three-way-catalyst (TWC) that is used in gasoline engines, due to the lower exhaust gas temperatures from a diesel engine. Temperature peaks, e.g. during soot regeneration of the DPF, do however arise and thermal deactivation of the DOC has to be considered. Sintering also includes agglomeration of active material and in this sense lowering the dispersion.

Less dispersion does not necessary imply less activity. A catalytic reaction is defined as *structure sensitive* if the rate changes markedly as the particle size of the catalyst is changed [11]. It has been suggested that the NO oxidation is structure sensitive with a higher turnover frequency for larger Pt particles than small [12, 13, 5]. Wiebenga et al. [5] also imply that there is an optimal particle size, between 5–10 nm, where the NO oxidation activity is at its peak. This can be explained by realizing that small particles are easier to oxidize and therefore larger Pt particles has higher activity for NO oxidation, but when the particles grow too large the low dispersion weighs in more than the resistance to oxidation. The reason that oxidized Pt particles give a decline in activity is because the presence of Pt oxides hinders NO adsorption [3].

There are many factors that affect sintering kinetics: temperature, atmosphere, metal type, metal dispersion, promoters/impurities and support surface area, texture and porosity [14]. Because of this it is very cumbersome to predict sintering phenomena with theoretical models.

1.4.1.1 Precious Metals

As Pt is regarded to have the highest oxidation activity (compared to Pd) it is necessary to include it in the DOC. Pt is however more sensitive to thermal degradation, but addition of Pd has proven to cause less agglomeration of active material [13]. In contrast to Pd, the oxidation activity of Pt is drastically reduced when in oxidized state, PtO, and the NO oxidation of the DOC is most affected by the Pt oxidation. The formation of PtO is most predominant in lean burn engines (e.g. diesel engines), due to the excess O_2 which is responsible for Pt oxidation [15]. NO_2 is also responsible for the oxidation of Pt, but concentrations below 200 ppm has no effect as an additional oxidant for Pt [16].

Some reports have shown that migration of precious metals is facilitated by sulfur [17, 18, 19]. Auvray and Olsson [18] contradictory claim that the NO oxidation is improved by the addition of sulfur. This can be true with short exposure to high content of sulfur. As stated there is a optimum dispersion for NO oxidation and if sulfur improves the mobility of precious metals then the dispersion might reach its optimum faster. Longterm sulfur exposure is however not favored as will be discussed in the next section.

1.4.2 Chemical Deactivation

Catalyst poisons are substances that inhibits the active sites for reaction and because of this lower the catalytic activity. Moldovan et al. [20] showed that the the dominating catalyst poisons in diesel engines are sulfur, phosphorous and zinc, where the two latter originates from the lubricants.

Sulfur is a potent catalyst poison that inhibits the active sites for reaction. Sulfur originates from the fuel or lubricants and even though ultra-low sulfur diesel (ULSD) is commonly used, low concentrations can affect the activity. Due to excess oxygen in the diesel engine the sulfur is oxidized to SO_2 and can be further oxidized to SO_3. The NO oxidation in the DOC is heavily affected by the amount sulfur present. Kröcher et al. [21] showed that the NO oxidation activity (at 270 °C) after 14 hours dropped to approximately 80 % of the initial activity with 7 ppm sulfur diesel and to 60 % with 37 ppm sulfur diesel. The sulfur poisoning can further be divided into three categories, namely, metal oxide sulfation, washcoat sulfation and SO_x interactions with H_2O [22].

1.4.2.1 Metal Oxide Sulfation

Metal oxide sulfation occurs when a metal oxide (e.g. PtO and PdO) reacts with SO_3 to form a metal sulfate. Pt is less sensitive to sulfur poisoning than Pd, due to that Pd is readily converted to PdO at lean burn conditions, which in turn can react into inactive $PdSO_4$. Although Pt is active for SO_2 oxidation, the formation of $PtSO_4$ is seldom seen [22]. However, inactive $PdSO_4$ can form, but the metal oxide sulfation of Pd can be slowed by using Al_2O_3 which acts like a scavenger for SO_x [21].

1.4.2.2 Washcoat Sulfation

Washcoat sulfation means that SO_x interacts with the washcoat. As Al_2O_3 (used in Scania vehicles) is very susceptible for SO_3 it functions as a protection for $PdSO_4$ formation. SO_3 reacts with Al_2O_3 to form $Al_2(SO_4)_3$ which causes blockage of the pores and covers its surface, leading to less activity of the catalyst [22]. The reaction is reversible (*Reaction* (R 1.4)) but the backward reaction requires temperatures around 730 °C which very seldom reached in a DOC [23]. Lower decomposition temperatures for $Al_2(SO_4)_3$ has also been reported [24].

$$Al_2O_3 + 3\,SO_3 \underset{730\,^\circ C}{\rightleftharpoons} Al_2(SO_4)_3 \qquad \text{(R 1.4)}$$

1.4.2.3 Interactions with H_2O

The exhaust gas contains a considerable amount of H_2O which can react with SO_3 to form H_2SO_4. The H_2SO_4 masks the surface and blocks active sites. Further it may react with the washcoat, causing irreversible damage to the catalyst, but this process is very slow [21].

1.5 Motivation

As reviewed in *Section* 1.4 there are many factors that can contribute to the aging of the DOC. The NO oxidation performance, which is an important feature of the DOC, is very sensitive to aging and vehicles that have the same mileage or operating hours do not necessarily have to experience the the same deactivation of the catalyst. Factors such as fuel quality (poisoning and fouling), maximum/mean exhaust gas temperature (thermal deactivation) and temperature cycling (thermal deactivation) are continuously logged and available in Scania's databases. If these can be correlated to the activity of the DOC, then the aging and NO oxidation performance can be estimated.

This would have several benefits, including service time interval estimation and a more optimal performance of the SCR-system described in *Section* 1.3.4.1.

1.6 Problem Definition

Over time the DOC loses its initial activity due to aging. This directly affects the oxidation performance, especially the ability to oxidize NO to NO_2. As the DOC serves the purpose of adjusting the NO_2 to NO ratio for optimizing the performance of the SCR-system the DOC's NO oxidation activity is of major importance. This master thesis aims to find an empirical and statistical method to estimate the NO oxidation activity of the DOC after aging.

The DOC examined in this thesis is a commercially available catalyst.

1.6.1 Working Hypotheses

Based on previous sections, the following working hypotheses were investigated:

i) There is an empirical correlation between NO oxidation performance for the DOC and its history with respect to thermal and sulfur exposure.

ii) There exist implicit aging affects that scales proportionally to sulfur and thermal deactivation.

Chapter 2

Method

One of the main difficulties with determining catalytic activity is to put results from various experiments on a common scale. In this study a kinetic model has been used to estimate the activity in each experiment. The kinetic model was previously developed to predict nominal NO oxidation performance for the tested catalysts. For each experiment, the result was compared with the prediction of the model. If the prediction was significantly lower than the observed activity, it was concluded that the catalyst had aged and the difference was used to quantify the aging. The model used to predict the NO oxidation activity is described in *Section* 2.1.2.

The main focus of the present study is to explore the connection between the observed aging and what the catalysts were subjected to with the goal of being able to predict catalyst aging based on available information. To do this the kinetic model was extended to include aging information. As described in the background, many factors can contribute to catalyst aging. Therefore, one important task is to determine which information that must be treated explicitly and which can be treated implicitly.

The model and the method to quantify aging will be described in this chapter. Data from two different runs were used to build the model; an accelerated cycle (high temperature) and a non-accelerated cycle (low temperature). The cycles are very different and should represent a wide range of driving conditions. A summary of the runs can be seen in *Table* 2.1 and a visualization of the temperature profiles are depicted in *Figures* 2.1 and 2.2. The runs as whole are also included in *Appendix* B.1.

The model was then applied to 4 different runs summarized in *Table* 2.2 in a bid to validate it. The cycles are depicted in *Figures* 2.3 to 2.6 and the whole runs are included in *Appendix* B.2.

Table 2.1: Summary of the accelerated cycle and the non-accelerated cycle used for modeling

Type	AVL Concerto™ protocol	Reference	Approximate total runtime	Platform
Non-accelerated	68784xxx.x	[25]	2000 h	D13
Accelerated	68783xxx.x	[26]	1100 h	D13

Table 2.2: Summary of the test bench engine cycles used for validation

Type	AVL Concerto™ protocol	Reference	Approximate total runtime	Platform
STD6	68777xxx.x	[27]	1100 h	D9
STD6	68755xxx.x	[28]	1100 h	D13
STD5	68720xxx.x	[29]	2000 h	D16
STD5	68719xxx.x	[30]	2000 h	D16

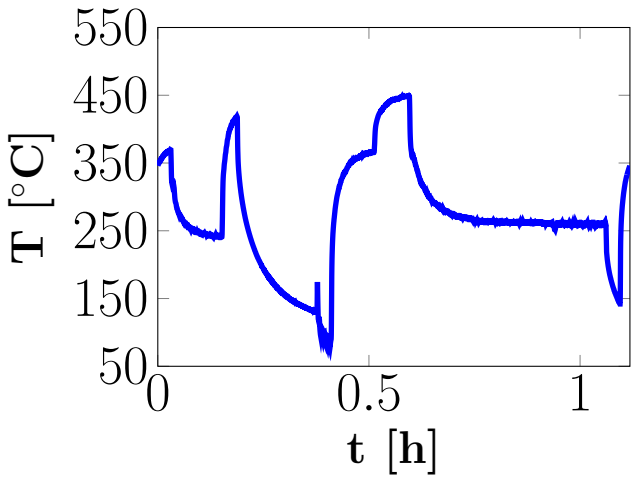

Figure 2.1: Temperature profile for the non-accelerated cycle.

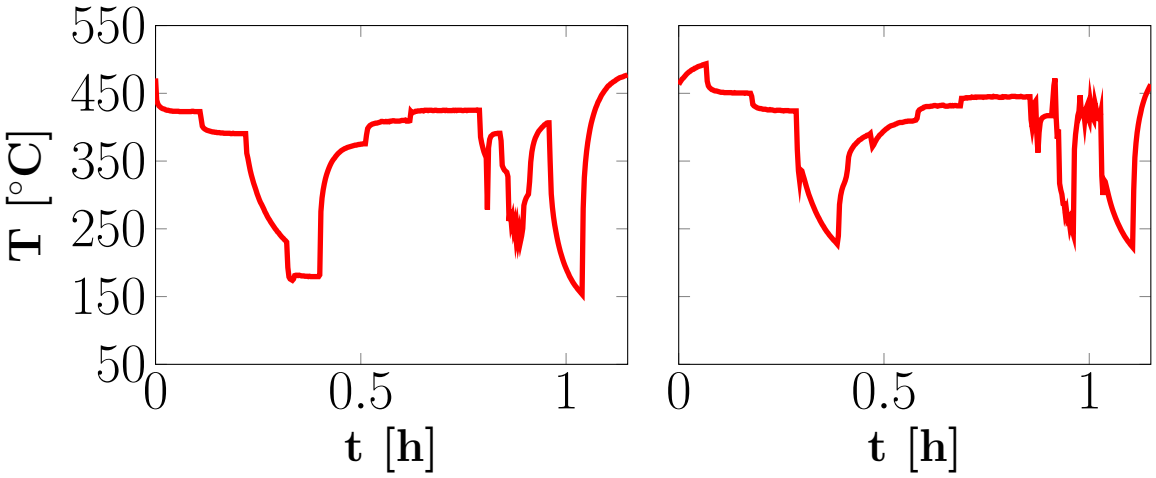

(a) Type I (b) Type II

Figure 2.2: Temperature profile for the accelerated cycle.

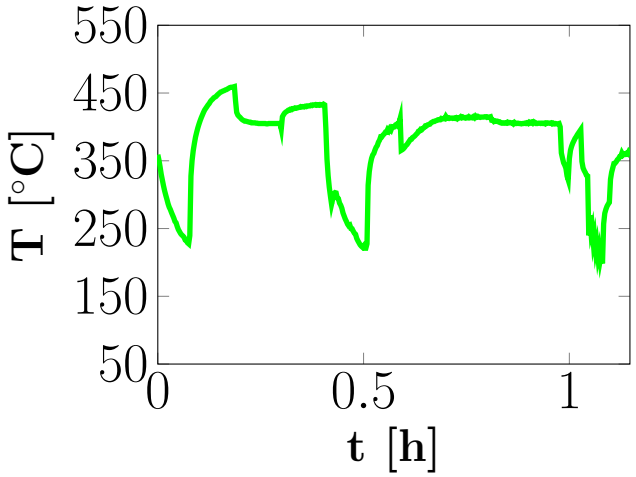

Figure 2.3: Temperature profile for validation cycle 68777xxx.x.

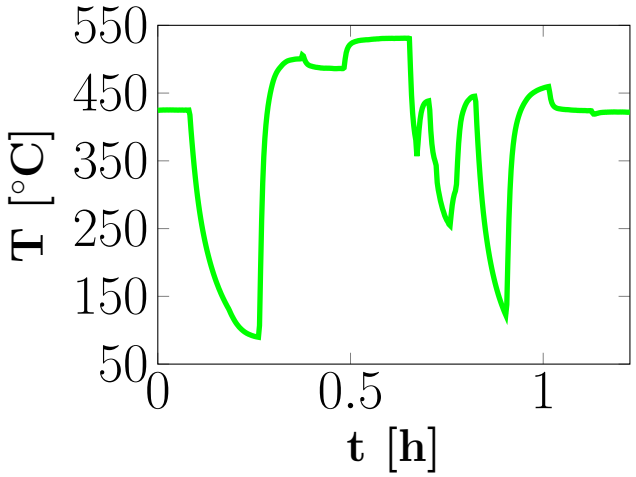

Figure 2.4: Temperature profile for validation cycle 68755xxx.x.

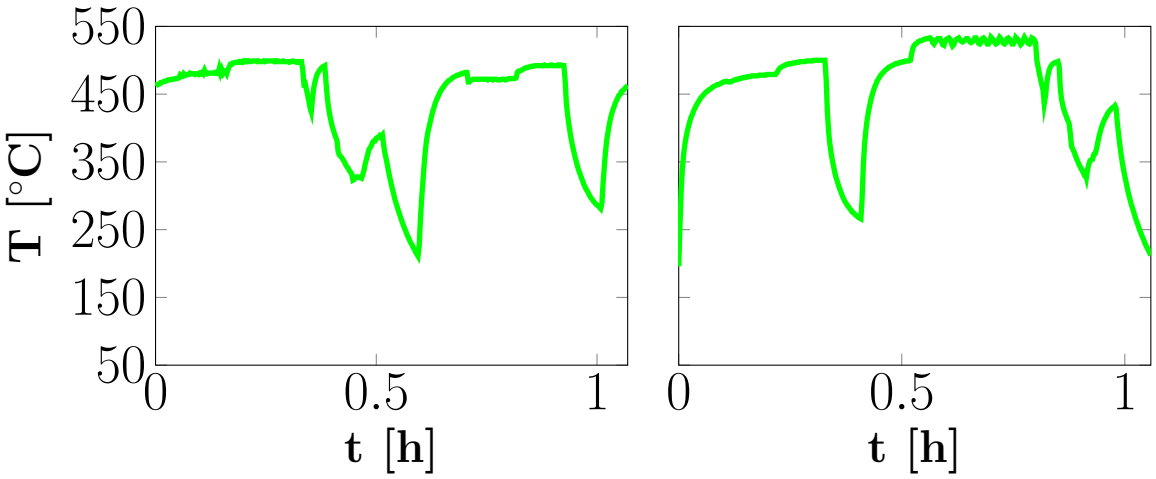

(a) Type I

(b) Type II

Figure 2.5: Temperature profile for validation cycle 68720xxx.x.

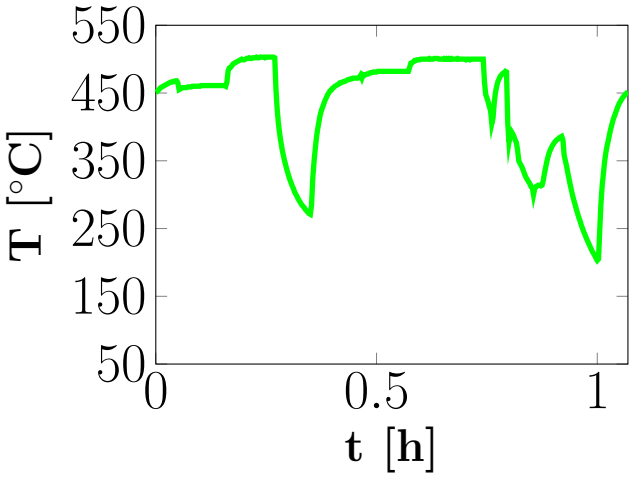

Figure 2.6: Temperature profile for validation cycle 68719xxx.x.

2.1 NO Oxidation

2.1.1 Thermodynamics

The NO oxidation is exothermic, i.e. the reaction is thermodynamically unfavored at higher temperatures where the thermodynamic constraint becomes significant. This includes the temperatures that may emerge in a diesel engine, especially over the DOC (see *Figure* A.1 in *Appendix* A).

If the change in total pressure is neglected (which is reasonable at the low concentrations of NO and NO_2 in the exhaust gas) the equilibrium relation ${}^{NO_2}/_{NO_x}$, f_{NO_2}, can be expressed as [31]:

$$f_{NO_2,eq} = \frac{p_{NO_2,eq}}{p_{NO_x}} = \frac{1}{1 + \frac{1}{K_p}\left(\frac{p_{ref}}{p_{O_2}}\right)^{0.5}} \tag{2.1}$$

p_{NO_2}, p_{NO_x} and p_{O_2} are partial pressures and p_{ref} is the reference pressure (1.01325 bar). The equilibrium constant, K_p, can be calculated according to [31, 32]:

$$K_p = \exp\left[\frac{5.8 \times 10^4 - 75.8T}{RT}\right] \tag{2.2}$$

where R is the gas constant ($8.3145\,\mathrm{J\,mol^{-1}\,K^{-1}}$) and T is the temperature in Kelvin. The partial pressure of O_2, p_{O_2}, is readily obtained through Dalton's law.

2.1.2 Kinetics

Higher temperatures are thermodynamically unfavorable for NO oxidation, but the kinetics are improved at higher temperatures. A general expression for the rate of reaction, r, can be witten as:

$$r = \underbrace{A}_{\text{I}} \underbrace{\exp\left[-\frac{E_a}{RT}\right]}_{\text{II}} \underbrace{[A]^a[B]^b \ldots [I]^i}_{\text{III}} \tag{2.3}$$

The notations can be interpreted as:

I) A measure of available precious metal for reaction.

II) Reaction path which is proportional to the activation energy.

III) Decided by gas composition and flow.

All these three factors contribute to the rate of reaction. A model for the kinetics of NO oxidation over a DOC has been derived semi-empirically by Westerberg [33]. It was concluded that the kinetics depended on flow rate, temperature and concentration of NO and O_2. It was found that there was a significant correlation between O_2 concentration and temperature and it was therefore omitted. The reaction rate constant, k $\left[\mathrm{h}^{-1}\right]$, can be expressed as:

$$k\tau = \underbrace{\exp\left[c_0\right]}_{\mathrm{I}} \times f\left(\underbrace{T, F, y_{\mathrm{NO}_x}}_{\mathrm{II,\ III}}\right) \tag{2.4}$$

where τ [h] is the residence time, T [K] is the temperature, F $\left[\mathrm{kg\,h}^{-1}\right]$ is the flow rate, y_{NO_x} is the mole fraction of NO_x and c_0 is a constant. The subscript ref refers to reference states. c_0 and other constants are obtained from experiments and multiple linear regression and are specific for each DOC. The underbraces are analogous to the notations in *Equation* (2.3). Treating the DOC as an ideal plug flow reactor with first order kinetics the conversion can be expressed as:

$$k\tau = -\ln\left[\frac{1-X}{1-X_f}\right] \tag{2.5}$$

where X_f is the conversion at inlet of the DOC and the conversion is defined as:

$$X = \frac{f_{\mathrm{NO}_2}}{f_{\mathrm{NO}_2,eq}} \tag{2.6}$$

From this model it is possible to estimate a deactivation factor for the DOC, ξ, which will be explained in *Section* 2.1.3.

2.1.3 Deactivation Factor

In *Section* 2.1.2, the kinetics for NO oxidation were reviewed. From this theory a deactivation factor of the DOC, ξ, can be estimated with the following assumptions:

i) The kinetics are described with *Equation* (2.4) and other parameters that might influence the kinetics are neglected.

ii) Flow, temperature and concentration (NO and O_2) affect the kinetics, but are not properties of the catalyst and hence the dependencies of these parameters are determined for a fresh catalyst but are constant as the catalyst ages.

iii) The only thing that influences the NO oxidation activity is the precious metal available for reaction. c_0 changes as the catalyst ages.

A ($\exp\left[c_0\right]$) is a measurement of the precious metal available for reaction and can directly be linked to the deactivation of the catalyst. The pre-factor A is scaled to account for deactivation. ξ is defined as:

$$\xi = \frac{A_{obs}}{A_{degr}} = \frac{\exp\left[c_{0,obs}\right]}{\exp\left[c_{0,degr}\right]} \tag{2.7}$$

Resulting in the final rate expression for an aged DOC:

$$k_{obs}\tau = \exp\left[c_{0,degr} + \ln\left[\xi\right]\right] \times f\left(T, F, y_{\mathrm{NO}_x}\right) \tag{2.8}$$

where *obs* stands for observed and *degr* for degreened. Hereafter, c_0 will be equivalent to $c_{0,degr}$.

2.2 Data Collection

2.2.1 Test Bench Engine

For collection of data, AVL Concerto™ was used. This program retrieves test bench engine data from a database called *PUMA*. Written scripts were used to collect and sort the parameters of interest. The parameters that were collected are presented in *Table* 2.3.

Table 2.3: Parameters collected from AVL Concerto™

Name	Description	Unit
HM03	Total runtime	h.min
TE09/TG21	Temperature DOC inlet	°C
NM00	Engine speed	rpm
QB00	Mass flow fuel	$\mathrm{mg\,h^{-1}}$
ξ	Activity	%

There exist two types of data for the parameters in *Table* 2.3. One with high time resolution (recorder) and one with low time resolution. To get best possible input data for the model the recorder was used. However, it only records a short period of time and therefore assumptions were made (the validity of using recorders to represent the whole runs is justified in *Appendix* C). For the cycles used to build the model:

i) The cycle in *Figure* 2.1 can be used to represent the whole run for 68784xxx.x (*Figure* B.1).

ii) The cycle in *Figure* 2.2a can be used to represent the first 350 h for 68783xxx.x (*Figure* B.2) and the cycle in *Figure* 2.2b can be used to represent the rest.

For the validation cycles:

i) The cycle in *Figure* 2.3 can be used to represent the whole run for 68777xxx.x (*Figure* B.3).

ii) The cycle in *Figure* 2.4 can be used to represent the whole run for 68755xxx.x (*Figure* B.4).

iii) The cycle in *Figure* 2.5b can be used to represent the time between 0–400 and 1400–1700 h for 68720xxx.x (*Figure* B.5) and the cycle in *Figure* 2.5a can be used to represent the rest.

iv) The cycle in *Figure* 2.6 with a y-shift of +15 °C can be used to represent the first 1400 h for 68719xxx.x (*Figure* B.2) and the cycle in *Figure* 2.6 can be used to represent the rest.

The mean mass flow of fuel was used. This was compared to using the momentary fuel consumption, but no huge difference was induced. This works for periodic test bench engine runs, but in real world applications the momentary fuel consumption must be used. The oil to fuel ratio was obtained from reports (same references given in *Tables* 2.1 and 2.2) and was assumed to be constant throughout the runs. The sulfur content of the diesel and oil was assumed to b 4 ppm and 3000 ppm, respectively.

2.2.2 Retrieval of Deactivation Factor

The calculation of ξ was performed with scripts in Concerto™ and Matlab that use the approach described in *Section* 2.1.3.

When measuring the NO oxidation of the DOC at Scania, there are several methods that are utilized, which give different output values for ξ. To get the best value for ξ, it was calculated as a mean of all available activity measurements at that specific time. As the model that calculates ξ is based on a reference DOC it is not exact. The activity differs especially for the measurement of a fresh catalyst as the activity changes fast in the beginning. Therefore all catalyst were assumed to start from activity of 100 % when building the model. By minimizing the sum of squared residuals between actual measurements and the model (*Equation* (2.8)) the values of ξ (*Table* 2.4) for the runs were obtained.

Table 2.4: Retrieved ξ at different times for the runs. Data are presented as deactivation factor ξ [%] at time t [h] ($t : \xi$)

AVL Concerto™ protocol	$t_1 : \xi_1$	$t_2 : \xi_2$	$t_3 : \xi_3$	$t_4 : \xi_4$	$t_5 : \xi_5$
68784xxx.x	0 : 94	621 : 78.6	1210 : 67.8	1737 : 56.7	2286 : 52.2
68783xxx.x	0 : 110	608 : 83.1	1189 : 67.6		
68777xxx.x	0 : 101	527 : 84.0	1242 : 70.3		
68755xxx.x	0 : 104	529 : 62	1085 : 35		
68720xxx.x	0 : 103	692 : 58.0	1177 : 41.8	1865 : 31.3	
68719xxx.x	0 : 108	503 : 73.7	938 : 54.4	1462 : 43.4	2043 : 37.5

Confidence intervals (95 %) for the values of ξ were obtained by calculating a new value for c_0 ($c_{0,obs}$) at the specific times in *Table* 2.4. With Matlab and *fitnlm.m*, confidence intervals for $c_{0,p}$ were obtained. By the definition of $c_{0,obs}$ (*Equation* (2.7)) the upper (u) and lower (l) boundary of the confidence interval is obtained:

$$\begin{aligned} \xi^u &= \exp\left[c_0 - c^u_{0,obs}\right] \\ \xi^l &= \exp\left[c_0 - c^l_{0,obs}\right] \end{aligned} \tag{2.9}$$

2.3 Thermal Load

When modeling for non-steady state temperature exposure, like in the DOC, it is desirable to transform the temperature exposure to one single temperature. It is done in this section and yields a quantified temperature exposure after time and is therefore easily comparable between different runs.

The sintering kinetics can be represented empirically by so called power laws. A Simple Power Law Expression (SPLE) has traditionally been used to predict the sintering behavior of catalysts [34]:

$$-\frac{d\left(D/D_0\right)}{dt} = k_s^{SPLE}\left(\frac{D}{D_0}\right)^n \tag{2.10}$$

D and D_0 is the dispersion and initial dispersion of active material, respectively. k_s is the sintering rate constant and n is the sintering order. Another approach is the General Power Law Expression (GPLE) [35]:

$$-\frac{d\left(D/D_0\right)}{dt} = k_s^{GPLE}\left(\frac{D}{D_0} - \frac{D_{eq}}{D_0}\right)^m \tag{2.11}$$

The difference with the GPLE is that D_{eq} is introduced to account for equilibrium dispersion at $t \to \infty$. D_{eq} is a function of temperature and cannot be calculated *a priori* [36, 37]. The sintering orders, n and m, ranges from 3–15 and 1–2, respectively [14].

As described in *Section* 1.4.1 the reason for a decline in activity due to thermal exposure is sintering, hence:

$$\frac{D}{D_0} \propto \xi \tag{2.12}$$

Equations (2.10) and (2.12) combined yield:

$$-\frac{d\xi}{dt} = k_s\xi^n \tag{2.13}$$

Separating variables, defining the boundaries and integrating, summarize to *Equations* (2.14) and (2.15):

$$-\int_{\xi_0=1}^{\xi}\frac{d\xi}{\xi^n} = \int_0^t k_s dt$$

$$\frac{1}{1-n}\left(\xi^{1-n} - 1\right) = -k_s t, \qquad n \neq 1 \tag{2.14}$$

$$\ln \xi = -k_s t, \qquad n = 1 \tag{2.15}$$

k_s is dependent on temperature and can be expressed by an Arrhenius expression:

$$k_s = -k_{s,0} \exp\left[-\frac{E_s}{RT}\right] \tag{2.16}$$

where E_s is the thermal deactivation energy. Since k_s is dependent on temperature, exposure to different temperatures induce more or less activity loss. Because of this it is hard to quantify the temperature exposure directly. The approach in this thesis is to apply *equivalent thermal exposure* [38]. The basic principle behind the idea is that the LHS of *Equations* (2.14) and (2.15) has the same value for different k_s and t on the RHS. In mathematical terms:

$$k_s(T_1)t_1 = k_s(T_2)t_2 = k_s(T_3)t_3 = \ldots = k_s(T_i)t_i \tag{2.17}$$

If a reference temperature of 550 °C (T_{ref}) is used it implies that for T_1 at time t_1:

$$k_s(T_i)t_i = k_s(T_{ref})t_{ref} \tag{2.18}$$

If a histogram with i bins describing the thermal exposure of the DOC is obtained, then the equivalent thermal load at T_{ref} can be calculated as:

$$\sum_i k_s(T_i)t_i = k_s(T_{ref})t_{550}$$

$$t_{550} = \frac{\sum_i k_s(T_i)t_i}{k_s(T_{ref}} \tag{2.19}$$

Inserting *Equation* (2.16) and assuming that $k_{s,0}$ is independent of temperature:

$$t_{550} = \frac{\sum_i \exp\left[-\frac{E_s}{RT_i}\right]t_i}{\exp\left[-\frac{E_s}{RT_{ref}}\right]} \tag{2.20}$$

t_{550} is a measure of the thermal load and can be used directly in the model. In this thesis, the bins were defined with a width of 10 °C and the temperature of each bin was defined as the mean of the edges. E_s was not calculated, but literature reports values between 30–150 kJ mol^{-1} [14], so it was assumed to be 100 kJ mol^{-1}.

2.4 Sulfur Poisoning

As discussed in the background, there are many interactions for the DOC with sulfur. To make it possible to investigate sulfur's impact on DOC's NO oxidation performance over time, sulfation and desulfation steps are treated as lumped models occurring at different temperatures. Sulfation and desulfation rates for a DOC is given by *Table* 2.5 and *Equation* (2.21). The sulfation rates are estimated from graphs and tables [39, 40, 41], and the desulfation rates are taken from [42].

Table 2.5: Sulfation rates at different temperatures and accumulated sulfur [39, 40, 41]. Sulfation rates are given as a sticking factor in %

m_S [g]	200 °C	250 °C	300 °C	400 °C	450 °C
0	XX[a]	XX[a]	XX[a]	XX[a]	XX[a]
2	XX[a]	XX[a]	XX[a]	XX[a]	XX[a]
6	XX[a]	XX[a]	XX[a]	XX[a]	XX[a]
8	XX[a]	XX[a]	XX[a]	XX[a]	XX[a]
10	XX[a]	XX[a]	XX[a]	XX[a]	XX[a]

[a] Values are left out intentionally.

$$k_{DS} = \mathrm{XX} \exp\left[-\frac{\mathrm{XX}}{T}\right], \qquad \text{(Constants are left out intentionally)} \tag{2.21}$$

Through interpolation in *Table* 2.5 and using *Equation* (2.21) the current reversible accumulated sulfur (S_R) in the DOC can be estimated after a given time. The approach is iterative, i.e. the sulfation history is needed to calculate the current reversible accumulated sulfur. However, as it is reversible it does not contribute to a permanent deactivation of the DOC. Owing to this reason, some assumptions are made:

i) The formation of sulfates can be seen as irreversible.

ii) The kinetics are dependent on the amount reversible accumulated sulfur.

iii) There is a maximum for the amount of irreversible accumulated sulfur.

The first assumption is justified by the high temperatures needed for the sulfates to decompose and these temperatures are not reached in the DOC. The second assumption is justified by that more reversible accumulated sulfur is equivalent to more available sulfur for sulfate formation. The third assumption is initially trivial as there cannot form more sulfates than available reactants. Less trivial is how much sulfates that can form before the resistance in mass transfer becomes too great. The proposed model for the irreversible accumulated sulfur is:

$$S_{IR} = S_{IR}^{max}\left(1 - \exp\left[-b\int \frac{dS_R}{dt}dt\right]\right) \tag{2.22}$$

In *Equation* (2.22) S_{IR}^{max} describes the maximum irreversible accumulated sulfur and b is a fitting constant. S_{IR}^{max} and b were estimated from Post Mortem Analysis (PMA) studies.

The input for the proposed sulfur accumulation model is the mean fuel consumption [mg h^{-1}] temperature [°C] (at specific times) and oil to fuel consumption ratio [%]. The model was evaluated in Matlab. In *Figure* 2.7 the reversible accumulated sulfur according to mapping data can be seen. It should be noted that steady-state (adsorption and desorption are in equilibrium) is reached fast and the amount of reversible accumulated sulfur is higher when the engine has run at lower temperatures. This is in agreement with previous experiments [39, 42]. It is assumed that S_{IR} is the sole cause of sulfur deactivation and S_R is neglected. This is of course not true, but the reversible sulfur can desorb and hence the highest possible NO oxidation at a specific time is considered.

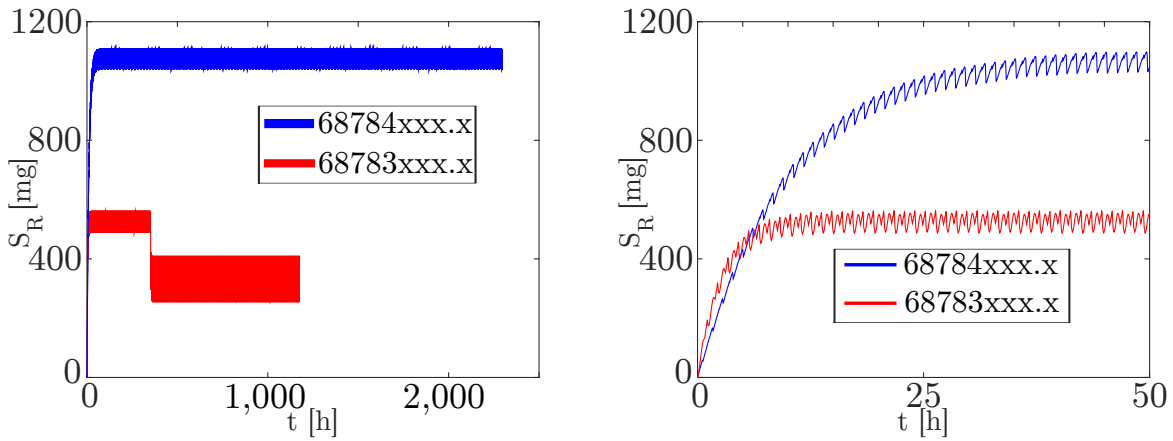

(a) Whole runs

(b) First 50 h

Figure 2.7: Reversible accumulated sulfur in DOC. Legend refers to Concerto protocol number.

2.5 Proposed Aging Model

It is evident that the NO oxidation activity drops in a negative exponential manner and hence the proposed general function to describe the NO oxidation activity is:

$$\xi = \alpha \exp\left[\beta\chi_1 + \gamma\chi_2 + \delta\chi_3 + \ldots + \psi\chi_i\right] + \omega \tag{2.23}$$

ξ is the NO oxidation activity (ideally 0 to 1), χ_i are functions describing any property of the system and α to ω are constants. Thermal and sulfur exposure were evaluated and other chemical deactivation mechanisms described in the background are assumed to be described implicitly by the sulfur exposure.

Chapter 3

Results and Discussion

3.1 Model Building

The input values to build the model are shown in *Table* 3.1.

Table 3.1: Input data for the model

AVL Concerto™ protocol	TE09 [°C]	QB00 [mg h^{-1}]	t_{550} at test end [h]	S_{IR} at test end [mg]
68784xxx.x	*Figure* 2.1	2.11×10^7	24.7	4.53×10^4
68783xxx.x	*Figure* 2.2	$3.91 \times 10^{7\,a}/3.92 \times 10^{7\,b}$	71.6	1.52×10^4

[a] First 350 h.
[b] After 350 h.

If it is assumed that sulfur accumulation and thermal exposure are the main causes of deactivation, *Equation* (2.23) is transformed into:

$$\xi = \alpha \exp\left[\beta S_{IR} + \gamma t_{550}\right] + \omega \tag{3.1}$$

Taking the natural logarithm yields:

$$\ln\left[\xi - \omega\right] = \ln\left[\alpha\right] + \beta S_{IR} + \gamma t_{550} \tag{3.2}$$

ω was set to 0.075, i.e. the lowest possible activity is 7.5 % of the original activity. This was chosen because the model expressed activity of 7–8 % before the DOC due to differing concentration of NO_2 at the DOC inlet. To achieve 100 % activity at $t = 0$, α is set to 0.925. The constants were achieved by fitting the data (*Table* 3.1) in a least square manner.

The result is visualized in *Figure* 3.1 and $\bar{R}^2$ is obtained from Matlab's *fitnlm.m*.

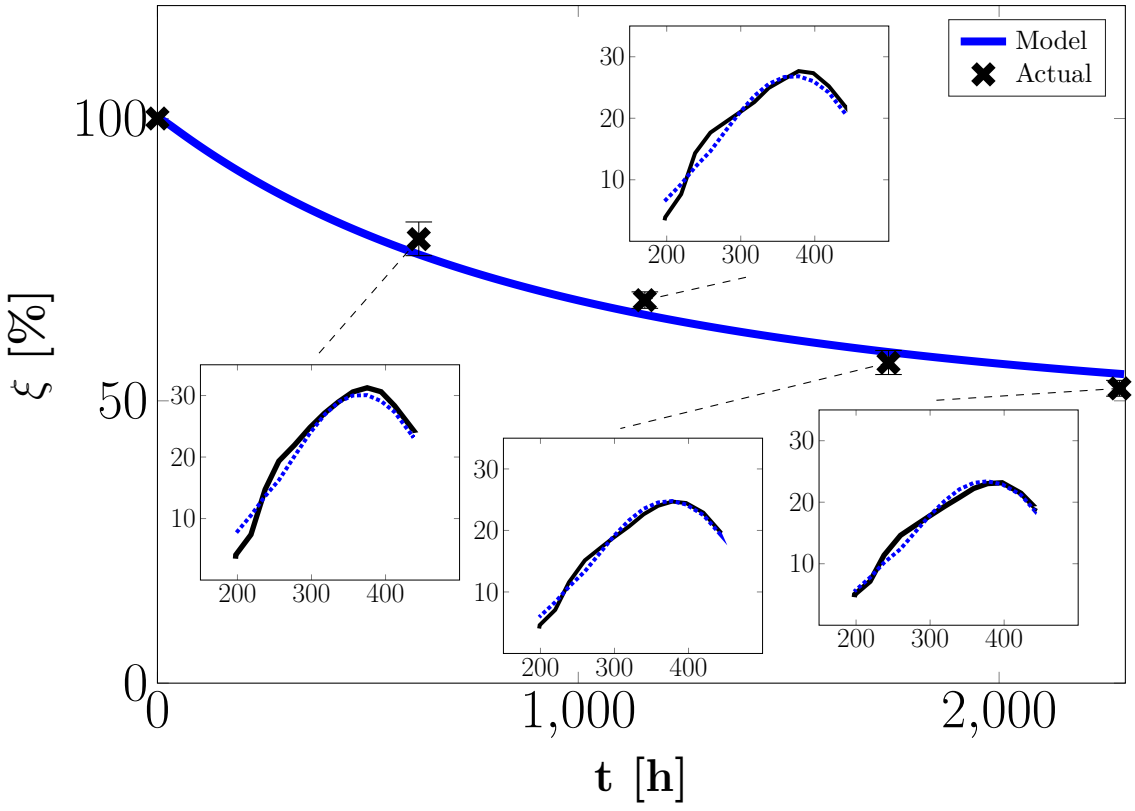

(a) 68784xxx.x

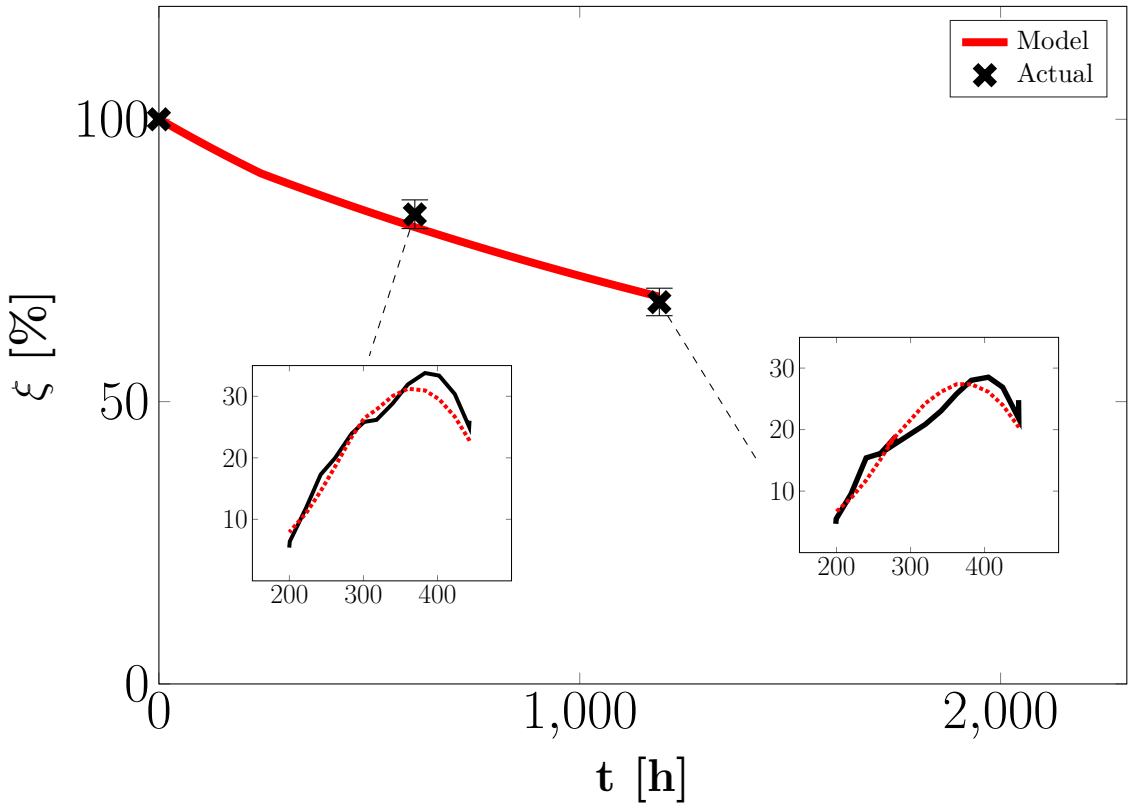

(b) 68783xxx.x

Figure 3.1: Actual and model NO oxidation activity as a function of time ($\bar{R}^2 = 0.985$). Subcaption refers to Concerto protocol number. Light-offs at a reference flow post DOC are provided at each experimental point as $\frac{NO2}{NO_x}$ [%] versus DOC inlet temperature [°C].

3.2 Model Validation

Table 3.2: Input data for the model validation

AVL Concerto™ protocol	TE09 [°C]	QB00 [mg h^{-1}]	t_{550} at test end [h]	S_{IR} at test end [mg]
68777xxx.x	*Figure* 2.3	3.12×10^7	47.4	2.01×10^4
68755xxx.x	*Figure* 2.4	4.81×10^7	195.1[a]	5.25×10^3
68720xxx.x	*Figure* 2.5	6.68×10^7	413.4	7.57×10^3
68719xxx.x	*Figure* 2.6	6.70×10^7	440.5	8.86×10^3

[a] Re-estimated to 342.5. See end of section.

When applying *Equation* (3.1) from *Section* 3.1, *Figures* 3.2 to 3.5 are obtained. Looking at *Figures* 3.1 to 3.5, it is noted that ξ asymptotically reaches a minimum. The minimum has two causes. The first cause is as described in the beginning of this chapter, that the model does not consider NO_2 at the inlet of the DOC. This is accounted for with ω being set to 0.075. However, it is evident that the gradient reaches zero at higher ξ than ω. Described in the method, GPLEs are commonly used as there is a minimum for dispersion which is dependent on temperature. This might be the cause of deviation at later times in the model. In addition the t_{550} for the model cycles are far less than the hot validation cycles and the model does not necessarily cover these high thermal loads.

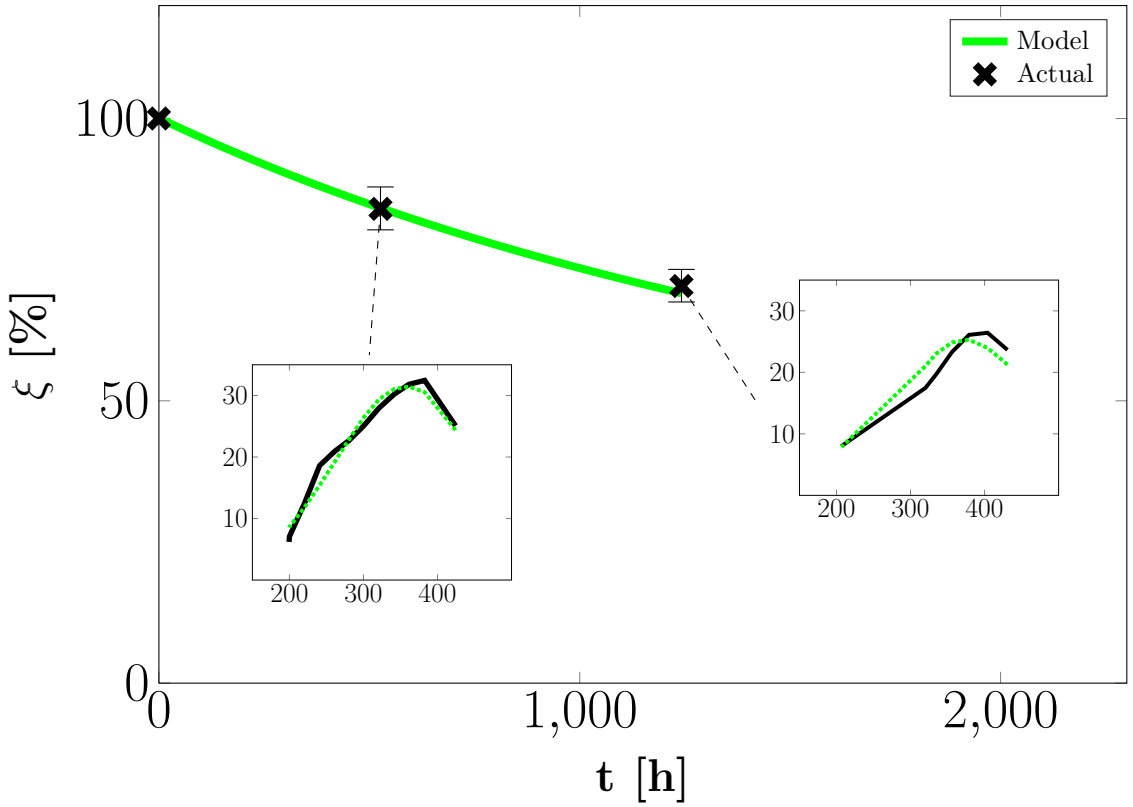

Figure 3.2: Activity versus time for 68777xxx.x. Light-offs at a reference flow post DOC are provided at each experimental point as $\frac{NO2}{NO_x}$ [%] versus DOC inlet temperature [°C].

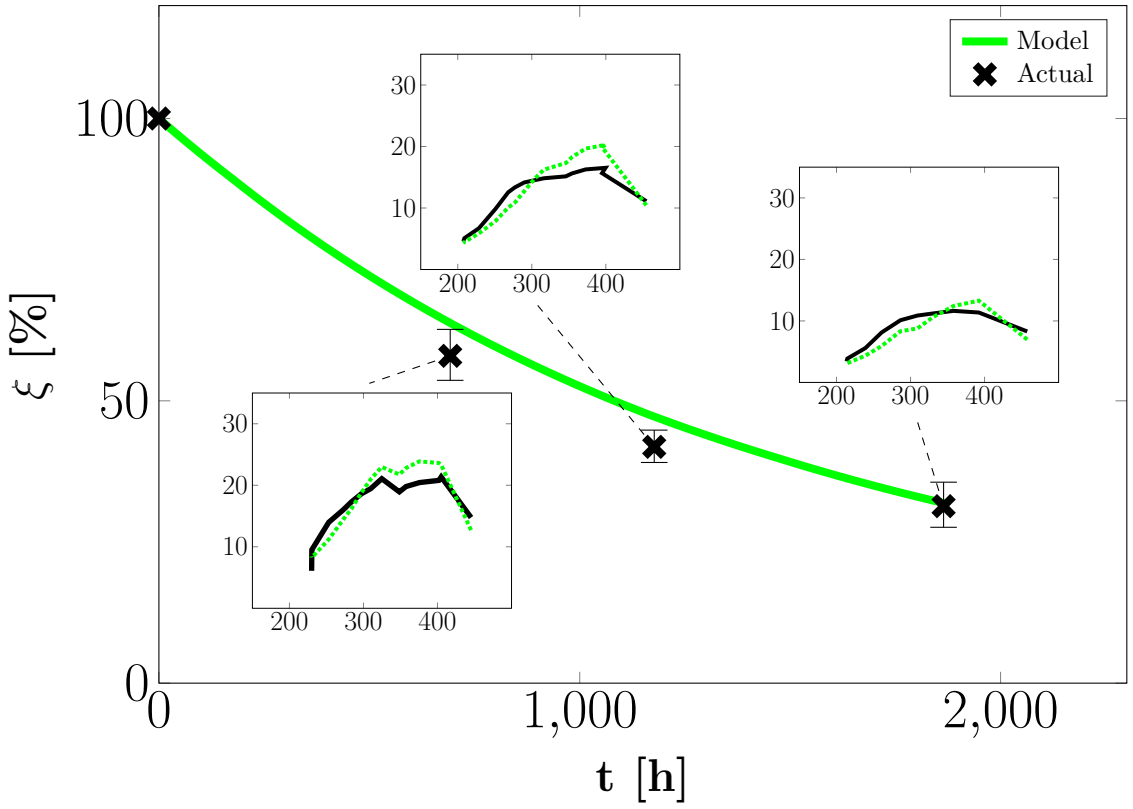

Figure 3.3: Activity versus time for 68720xxx.x. Light-offs at a reference flow post DOC are provided at each experimental point as $\frac{NO2}{NO_x}$ [%] versus DOC inlet temperature [°C].

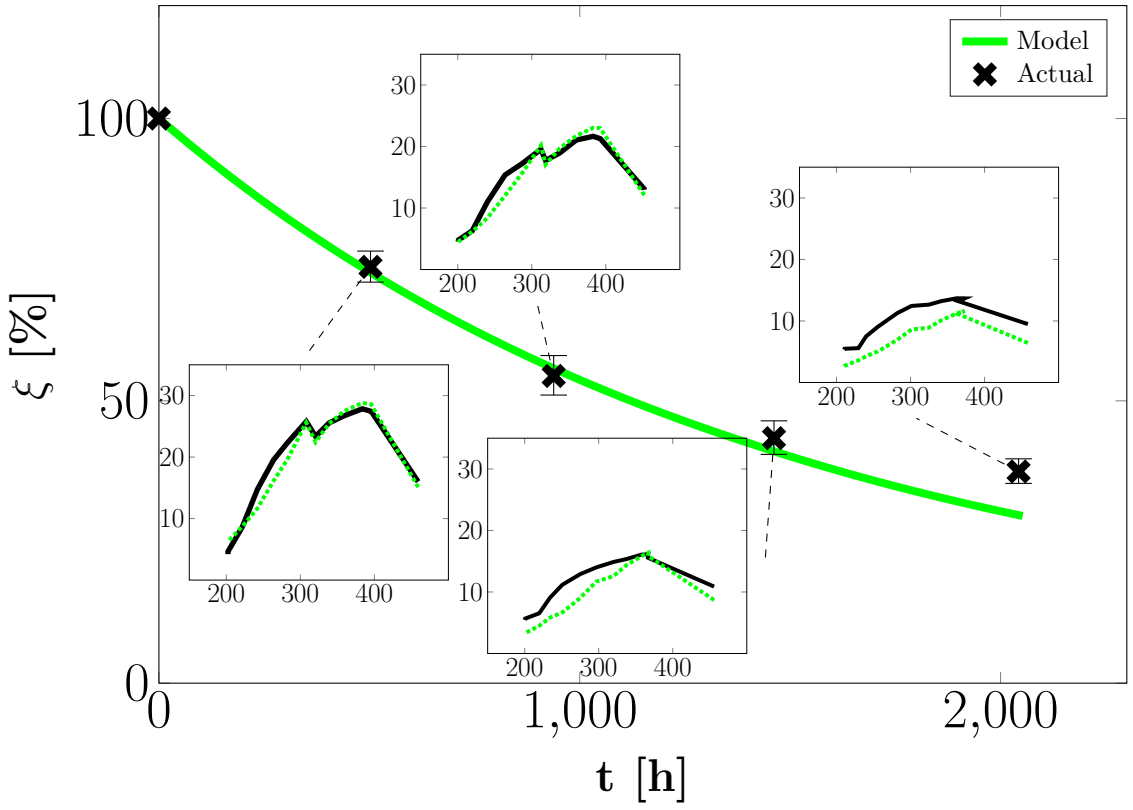

Figure 3.4: Activity versus time for 68719xxx.x. Light-offs at a reference flow post DOC are provided at each experimental point as $\frac{NO2}{NO_x}$ [%] versus DOC inlet temperature [°C].

When comparing the t_{550} in *Tables* 3.1 and 3.2 (pages 19 and 21) with the calculated values for HK01 (analogous to t_{550} but over the SCR which is calculated in the runs) in *Table* B.1 (page 32) it is in good agreement, with the exception of the t_{550} for 68755xxx.x, which value deviates. When collecting data for the run, a 250 h period was missing in the beginning and the temperature profile is not known in this part. If the same ratio is expected between 68719xxx.x and 68755xxx.x for t_{550} and HK01, t_{550} can be re-estimated as:

$$t_{550}(68755xxx.x) = \frac{t_{550}(68719xxx.x)}{\frac{\text{HK01}(68719xxx.x)}{\text{HK01}(68755xxx.x)}} = \frac{440.5}{\frac{319}{248}} = 342.5$$

If this instead is used and assumed to increase linearly from 0 to 342.5, *Figure* 3.5 is obtained which is in good agreement with the model.

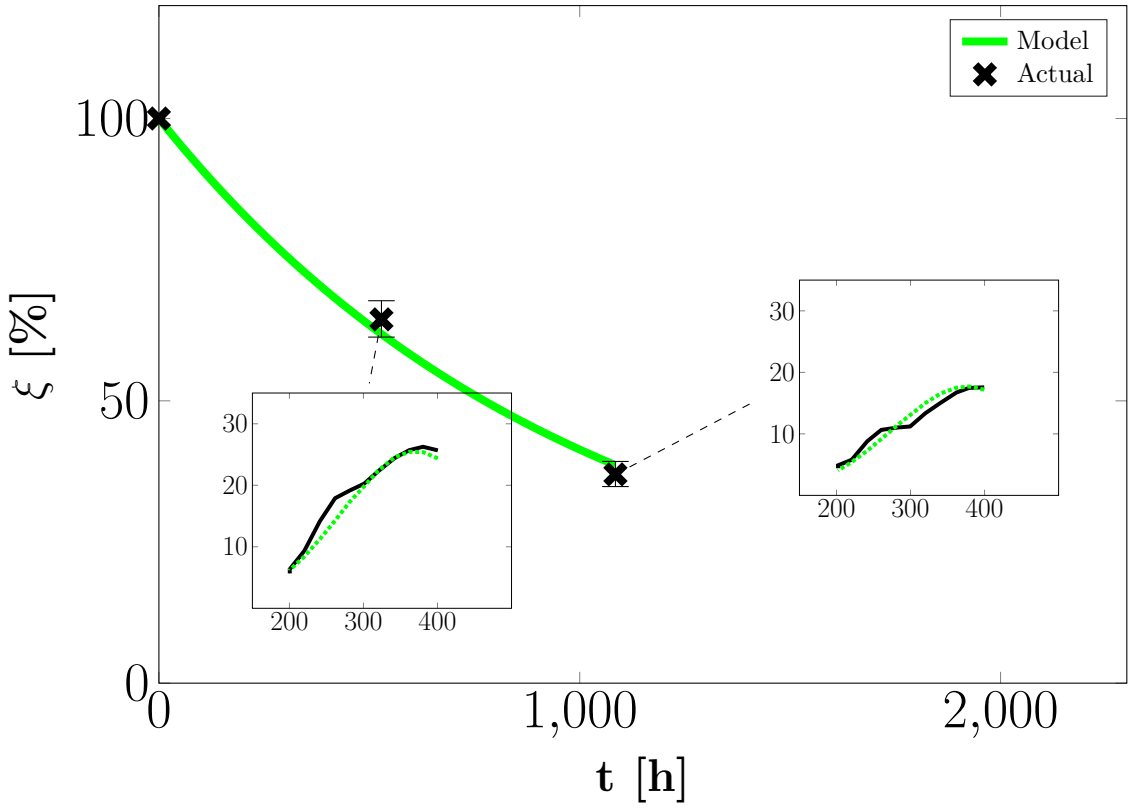

Figure 3.5: Activity versus time for 68755xxx.x. Light-offs at a reference flow post DOC are provided at each experimental point as $\frac{NO2}{NO_x}$ [%] versus DOC inlet temperature [°C].

3.3 Variation of Assumptions

Parameters that were implemented in the model based on assumptions were varied to see the influence on the outcome. The three parameters varied were the thermal deactivation energy, E_s, the sulfur content in fuel and the sulfur content in oil. Variation was done with one parameter at a time with ±25 % for E_s and sulfur content in oil and 0–10 ppm sulfur content in fuel. E_s was assumed to be 100 kJ mol^{-1}. Sulfur content in fuel was assumed to be 4 ppm. Sulfur content in oil was assumed to be 3000 ppm.

The only parameter that influences the outcome to some extent is E_s (*Figure* 3.6). This is expected for the hotter runs as the model cycles used were significantly cooler than these. The variation for the outcome is however not too large and does cover the 95 % confidence interval for the measurements. Varying sulfur content is captured when fitting the model and does not affect the result (see *Appendix* D).

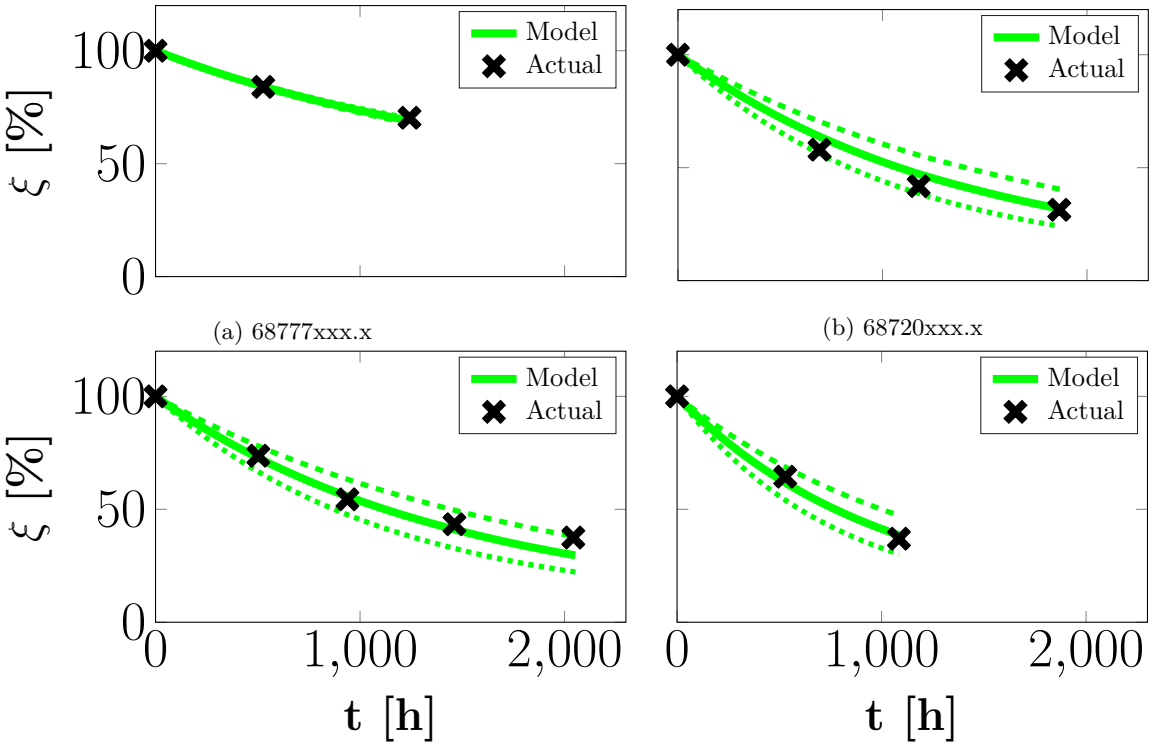

(a) 68777xxx.x

(b) 68720xxx.x

(c) 68719xxx.x

(d) 68755xxx.x

Figure 3.6: Variation of E_s where dashed and dotted line represent $75\,\mathrm{kJ\,mol^{-1}}$ and $125\,\mathrm{kJ\,mol^{-1}}$, respectively. Subcaption refers to Concerto™ protocol.

Chapter 4

Conclusions

The study shows that it is possible to predict NO oxidation activity for a DOC through empirical relations with thermal and sulfur exposure. The aging can to a large extent be explained by the test bench engine cycle it has been used on. As sulfur and thermal exposure are the only inputs, it implies that other deactivation mechanisms are described implicitly by these two deactivation mechanisms.

4.1 Future Work and Recommendations

The model describes how the DOC ages, but the NO oxidation also occurs over the DPF and could be extended to study DPF aging as well.

For most runs studied in this thesis, ξ seemed to stabilize after time. This might be an evidence for the existence of a minimum activity. It also seems to vary from one run to another, with $\frac{d\xi}{dt}$ reaching 0 faster at higher ξ when the temperature is low. It may imply that the lowest activity is temperature dependent and is recommended to study further. The model should also be extended to take into account the NO_x composition that enters the DOC.

The model used in this thesis to describe NO oxidation predicts the actual oxidation satisfactory at moderate to high temperatures ($> 250\,^{\circ}C$) with random variations. At lower temperatures the model systematically overpredicts the oxidation. A suggestion is to perform a temperature correction of the model by investigating the systematic deviation between model data and measured data as a function of temperature and continuously updating the model with new measurements of fresh DOCs.

The sulfur accumulation model presented in this thesis is based on adsorption/desorption data and three PMA studies. The function used provides a maximum value. This value does not necessarily explicitly describe the maximum irreversibly accumulated sulfur due to the fact that implicit chemical deactivation was assumed. However, sulfur is probably the main cause of chemical deactivation and its accumulation correlated to DOC deactivation can be further investigated.

For the fruitfulness of this study the possibility to apply the model on field trucks should be investigated. Some attempts were tried during the work but the data needed was not found.

References

[1] R. M. Heck, R. J. Farrauto, and S. T. Gulati. *Catalytic air pollution control: Commercial technology.* John Wiley & Sons Inc., 3rd edition, 2009.

[2] W. A. Majewski. What are diesel emissions. Technical report, DieselNet, 2012.

[3] A. Russell and W. S. Epling. Diesel oxidation catalysts. *Catal. Rev. - Sci. Eng.*, 53:337–423, 2011.

[4] Z. Yang, N. Zhang, Y. Cao, M. Gong, M. Zhao, and Y. Chen. Effect of yttria in Pt/TiO_2 on sulfur resistance diesel oxidation catalysts: Enhancement of low-temperature activity and stability. *Catal. Sci. Technol.*, 4:3032–3043, 2014.

[5] M. H. Wiebenga, C. H. Kim, S. J. Schmieg, S. H. Oh, D. B. Brown, D. H. Kim, J. Lee, and C. H. F. Peden. Deactivation mechanisms of Pt/Pd-based diesel oxidation catalysts. *Catal. Today*, 184: 197–204, 2012.

[6] J. B. Heywood. *Internal Combustion Engine Fundamentals.* McGraw-Hill Inc., 1988.

[7] W. A. Majewski. Urea dosing and injection systems. Technical report, DieselNet, 2014.

[8] H. Q. Wang, G. M. Liu, N. S. Peng, T. Feng, J. F. Xia, D. Y. Jiang, and X. C. Yang. Effect of NO_2 concentration on sensitivity for high temperature impedancemetric NO_x sensors. *Key Eng. Mat.*, 544: 372–375, 2013.

[9] T. C. Watling, M. Ahmadinejad, M. Ţuţuianu, Å Johansson, and M. A. J. Paterson. Development and validation of a Pt-Pd diesel oxidation catalyst model. *SAE Int. J. Engines*, 5:1420–1442, 2012.

[10] C. H. Bartholomew. Catalyst deactivation and regeneration. In *Kirk-Othmer Encyclopedia of Chemical Technology.* John Wiley & Sons Inc., 2000.

[11] G. A. Somorjai. *Introduction to surface chemistry and catalysis.* John Wiley & Sons Inc., 1994.

[12] O. K. Ezekoye, A. R. Drews, H. Jen, R. J. Kudla, R. W. McCabe, M. Sharma, J. Y. Howe, L. F. Allard, G. W. Graham, and X. W. Pan. Characterization of alumina-supported Pt and Pt–Pd NO oxidation catalysts with advanced electron microscopy. *J. Catal.*, 280:125–136, 2011.

[13] G. W. Graham, H. Jen, O. Ezekoye, R. J. Kudla, W. Chun, X. Q. Pan, and R. W. McCabe. Effect of alloy composition on dispersion stability and catalytic activity for NO oxidation over alumina-supported Pt–Pd catalysts. *Catal. Lett.*, 116:1–8, 2007.

[14] C. H. Bartholomew. Mechanisms of catalyst deactivation. *Appl. Catal., A*, 212:17–60, 2001.

[15] K. Hauff, W. Boll, S. Tischer, D. Chan, U. Tuttlies, G. Eigenberger, O. Deutschmann, and U. Nieken. Macro- and microkinetic simulation of diesel oxidation catalyst: Effect of aging, noble metal loading and platinum oxidation. *Chem. Ing. Tech.*, 85:673–685, 2013.

[16] K. Hauff, U. Tuttlies, G. Eigenberger, and U. Nieken. Platinum oxide formation and reduction during NO oxidation on a diesel oxidation catalyst – Experimental results. *Appl. Catal., B*, 123–124:107–116, 2012.

[17] X. P. Auvray, T. Pingel, E. Olsson, and L. Olsson. The effect gas composition during thermal aging on the dispersion and NO oxidation activity over Pt/Al_2O_3 catalysts. *Appl. Catal., B*, 129:517–527, 2013.

[18] X. P. Auvray and L. Olsson. Sulfur dioxide exposure: A way to improve the oxidation catalyst performance. *Ind. Eng. Chem. Res.*, 52:14556–14566, 2013.

[19] J. M. Jones, V. A. Dupont, R. Brydson, D. J. Fullerton, N. S. Nasri, A. B. Ross, and A. V. K. Westwood. Sulphur poisoning and regeneration of precious metal catalysed methane combustion. *Catal. Today*, 81:586–601, 2003.

[20] M. Moldovan, S. Rauch, G. M. Morrison, M. Gómez, and M. A. Palacios. Impact of ageing on the distribution of platinum group elements and catalyst poisoning elements in automobile catalysts. *Surf. Interface Anal.*, 35:354–359, 2003.

[21] O. Kröcher, M. Widmer, M. Elsener, and D. Rothe. Adsorption and desorption of SO_x on diesel oxidation catalysts. *Ind. Eng. Chem. Res.*, 48:9847–9857, 2009.

[22] H. N. Sharma, S. L. Suib, and A. B. Mhadeshwar. Interactions of sulfur oxides with diesel oxidation catalysts (DOCs). In *NOVEL MATERIALS FOR CATALYSIS AND FUELS PROCESSING*, pages 117–155, 2013.

[23] J. P. Breen, R. Burch, C. Hardacre, C. J. Hill, B. Krutzsch, B. Bandl-Konrad, E. Jobson, L. Cider, P. G. Blakeman, L. J. Peace, M. V. Twigg, M. Preis, and M. Gottschling. An investigation of the thermal stability and sulphur tolerance of Ag/γ-Al_2O_3 catalysts for the SCR of NO_x with hydrocarbons and hydrogen. *Appl. Catal., B*, 70:36–44, 2007.

[24] Y. Pelovski and V. Petkova. Mechanism and kinetics of inorganic sulphates decomposition. *J. Therm. Anal.*, 49:1227–1241, 1997.

[25] K. Erwe. Technical report, Scania CV AB, 2014. 7026086.

[26] K. Erwe and S. Svedberg. Technical report, Scania CV AB, 2014. 7026077.

[27] X. Karatzas and J. Karlgrund. Technical report, Scania CV AB, 2014. 7027567.

[28] S. Svedberg and K. Erwe. Technical report, Scania CV AB, 2014. 7024361.

[29] C. Öfverholm and T. Holmberg. Technical report, Scania CV AB, 2014. 7022145.

[30] C. Öfverholm and T. Holmberg. Technical report, Scania CV AB, 2014. 7022063.

[31] P. W. Atkins and J. de Paula. *Physical Chemistry*. Oxford University Press, 9th edition, 2010.

[32] R. J. Kee, F. M. Rupley, E. Meeks, and J. A. Miller. *Chemkin–III: A Fortran Chemical Kinetics Package for the Analysis of Gasphase Chemical and Plasma Kinetics*. Sandia National Laboratories, 1996.

[33] B. Westerberg. Technical report, Scania CV AB, 2012. 7013750.

[34] E. Ruckentein and B. Pulvermacher. Kinetics of crystallite sintering during heat treatment of supported metal catalysts. *AIChE J.*, 19:356–364, 1973.

[35] G. A. Fuentes. Catalyst deactivation and steady-state activity: A generalized power-law equation model. *Appl. Catal.*, 15:33–40, 1985.

[36] C. H. Bartholomew. Sintering kinetics of supported metals: New perspectives from a unifying GPLE treatment. *Appl. Catal., A*, 107:1–57, 1993.

[37] K. Nagashima and M. Nagata. Modeling of catalyst sintering and study of accelerated aging based on Pt/Al_2O_3 as a model catalyst. Technical report, SAE, 2007. 2007-01-1134.

[38] Environmental Protection Agency Federal Register. 40 CFR Part 86 Emission durability procedures and component durability procedures for new light-duty vehicles, light-duty trucks and heavy-duty vehicles; Final rule and proposed rule, Part IV, 2006.

[39] M. Skintemo. Technical report, Scania CV AB, 2011. 7006246.

[40] D. Raymand. Technical report, Scania CV AB, 2012. 7013995.

[41] D. Öqvist. Technical report, Scania CV AB, 2013. 7018647.

[42] D. Raymand. Technical report, Scania CV AB, 2012. 7010614.

[43] K. Erwe. Technical report, Scania CV AB, 2015. 7025223.

[44] X. Karatzas. Technical report, Scania CV AB, 2015. 7027693.

Nomenclature

E_s	Thermal deactivation energy.
F	Flow rate.
K_p	Equilibrium constant.
R	Gas constant.
T	Temperature.
τ	Residence time.
ξ	Deactivation factor.
c_i	Constant.
$f_{\mathrm{NO_2}}$	Ratio between $p_{\mathrm{NO_2}}$ and p_{NO_x}.
k	Reaction rate constant.
k_s	Sintering rate constant.
$p_{\mathrm{NO_2}}$	Partial pressure of $\mathrm{NO_2}$.
p_{NO_x}	Partial pressure of NO_x.
$p_{\mathrm{O_2}}$	Partial pressure of $\mathrm{O_2}$.
r	Rate of reaction.
ref	Reference state.
y_{NO_x}	Mole fraction of NO_x.
HK01	Thermal load for the SCR.
HK02	Chemical load (oil).
HK03	Chemical load (fuel).

Abbreviations

ANR	NH_3 to NO_x ratio.
ASC	Ammonia Slip Catalyst.
DOC	Diesel Oxidation Catalyst.
DPF	Diesel Particulate Filter.
EATS	Exhaust gas After Treatment System.
ECU	Electric Control Unit.
GPLE	General Power Law Expression.
HC	Hydrocarbon.
PM	Particulate Matter.
PMA	Post Mortem Analysis.
PN	Particulate Number.
SCR	Selective Catalytic Reduction.
SPLE	Simple Power Law Expression.
UDS	Urea Dosing System.
WHSC	World Harmonized Stationary Cycle.
WHTC	World Harmonized Transient Cycle.

Appendix A

NO Oxidation Equilibrium

The curves in *Figure* A.1 are obtained with *Equation* (2.1) and concern the reaction: The equilibrium reaction between NO and NO_2 is:

$$NO + \frac{1}{2} O_2 \rightleftharpoons NO_2 \tag{R A.1}$$

The equilibrium is dependent on temperature, moderately dependent on partial pressure of O_2 and slightly dependent on total pressure.

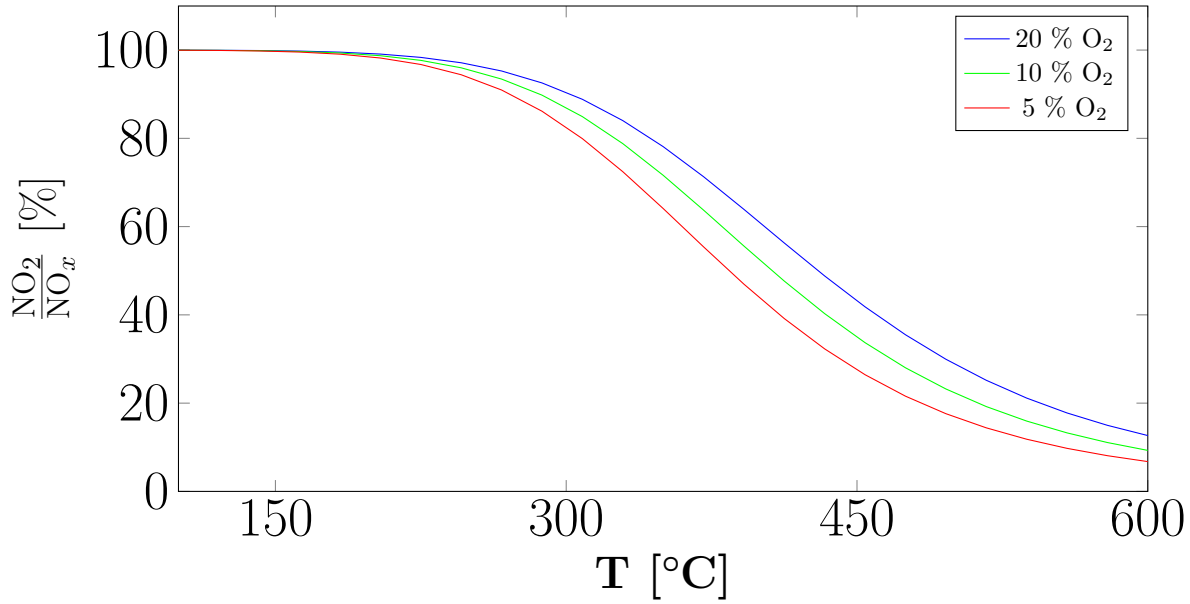

Figure A.1: NO oxidation thermodynamic equilibrium curves.

Appendix B

Test Bench Engine Summary

Figures B.1 to B.6 show the overall temperature through the whole runs. This is to visualize changes through the run. The missing fragments in each figure was assumed to resemble the surrounding profile. A summary of aging parameters is shown in *Table* B.1. HK01 (thermal load), HK02 (oil) and HK03 (fuel) are parameters that can have an influence on the deactivation of the DOC. They are set at Scania so that a number represent one life-time (70×10^6 km), i.e. HK01 = 100 h@550 °C, HK02 = 150 L and HK03 = 210 000 L represent 100 % for each parameter.

Table B.1: Test bench engine aging parameters

AVL Concerto™ protocol	HK01 [%]	HK02 [%]	HK03 [%]	Reference
68784xxx.x	27	17	26	[25]
68783xxx.x	60	20	26	[26]
68777xxx.x	44	20	22	[27]
68755xxx.x	248	19	21	[28]
68720xxx.x	275	63	47	[29]
68719xxx.x	319	73	54	[30]
68742xxx.x	121	25	24	[43]
68710xxx.x	27	29	27	[44]

B.1 Model Cycles

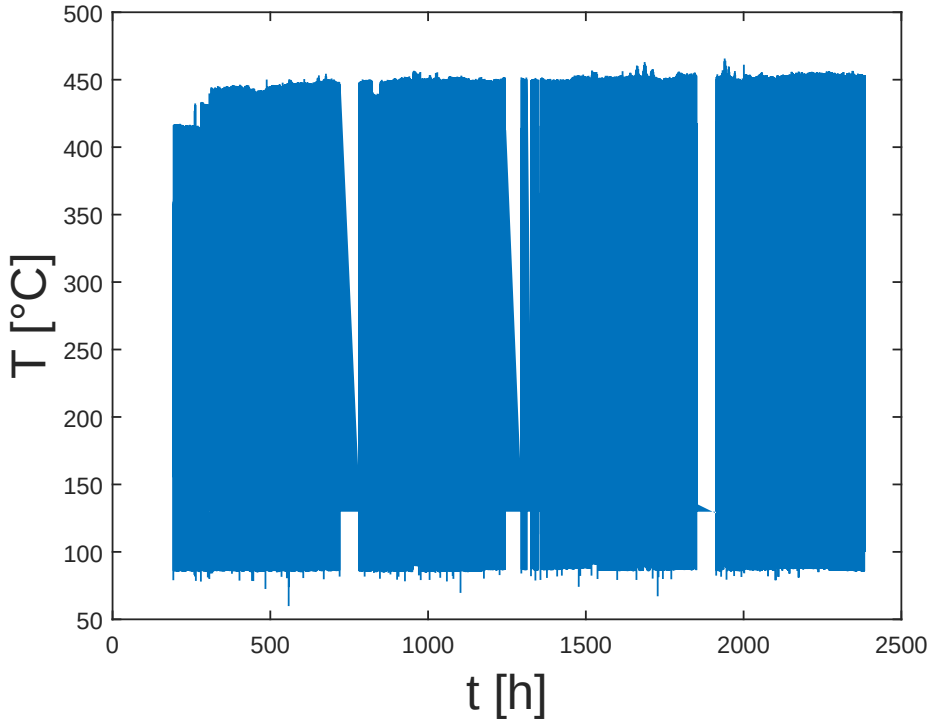

Figure B.1: Whole test bench engine temperature profile for 68784xxx.x.

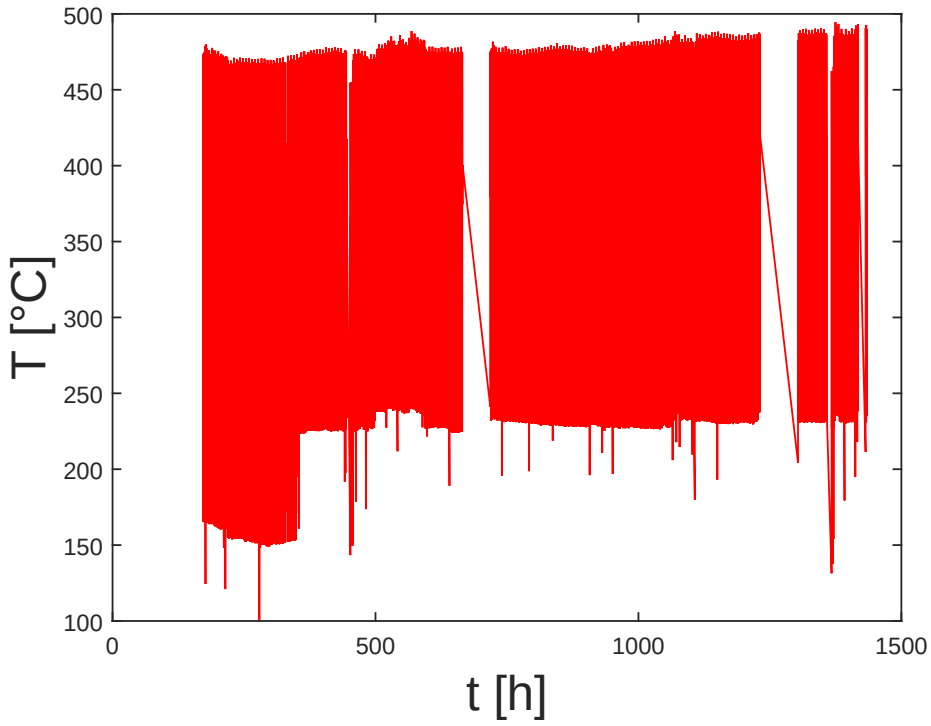

Figure B.2: Whole test bench engine temperature profile for 68783xxx.x.

B.2 Validation Cycles

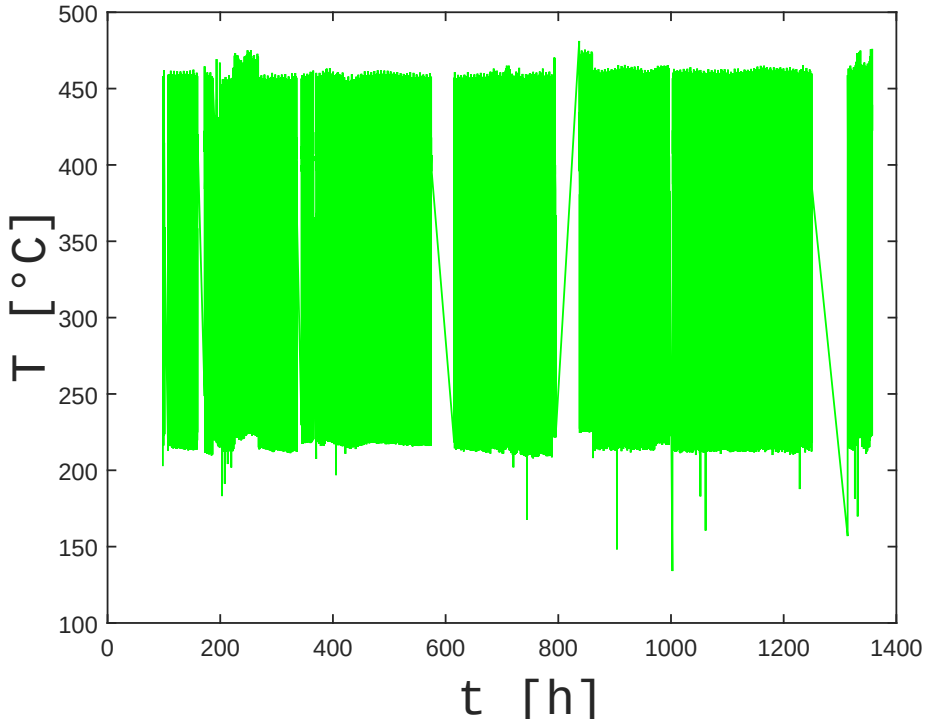

Figure B.3: Whole test bench engine temperature profile for 68777xxx.x.

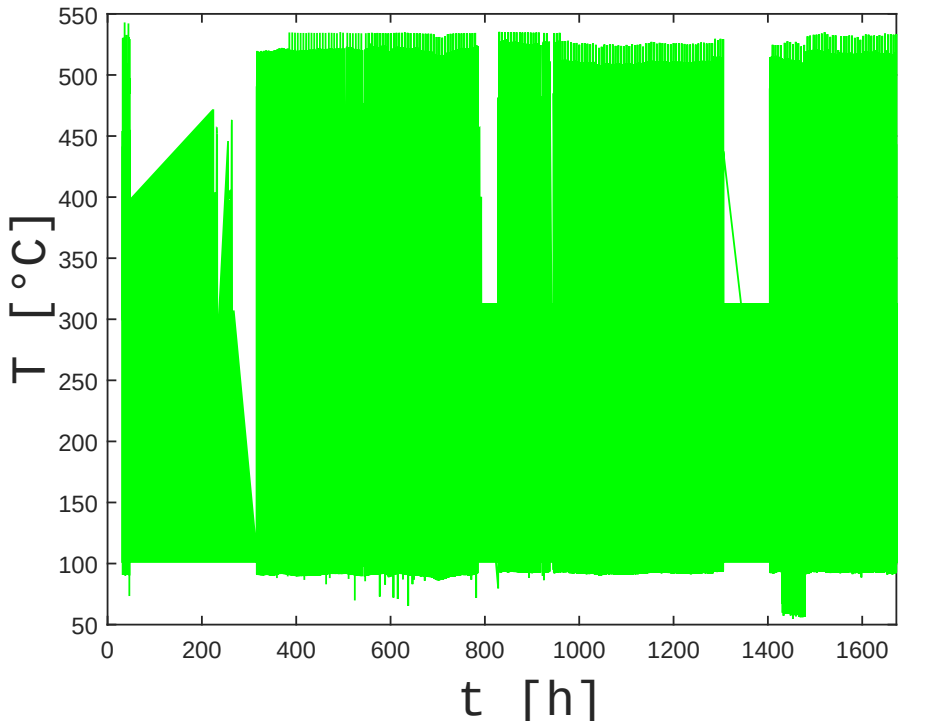

Figure B.4: Whole test bench engine temperature profile for 68755xxx.x.

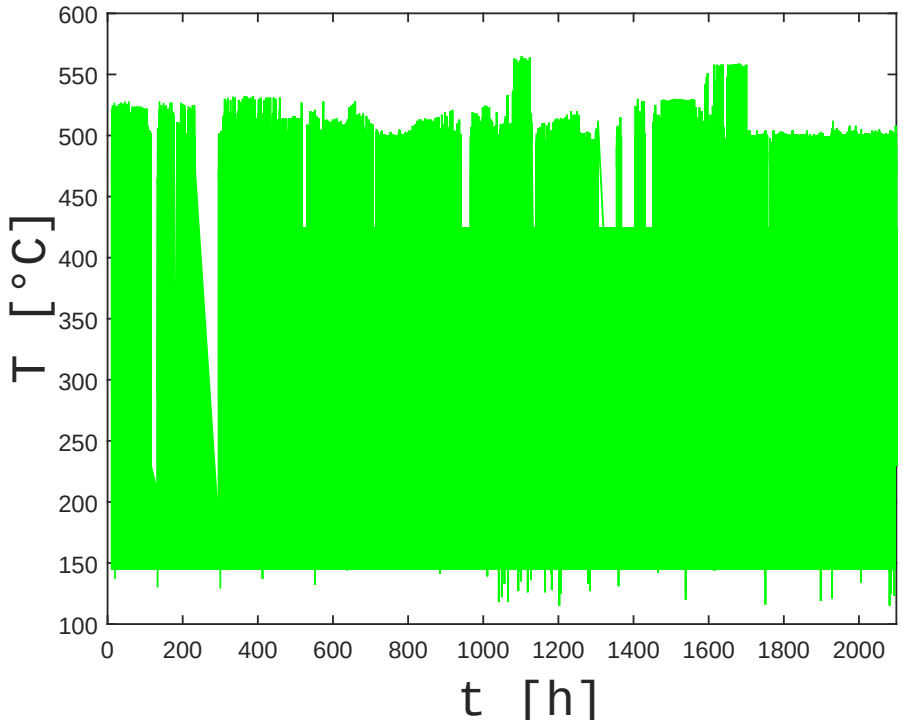

Figure B.5: Whole test bench engine temperature profile for 68720xxx.x.

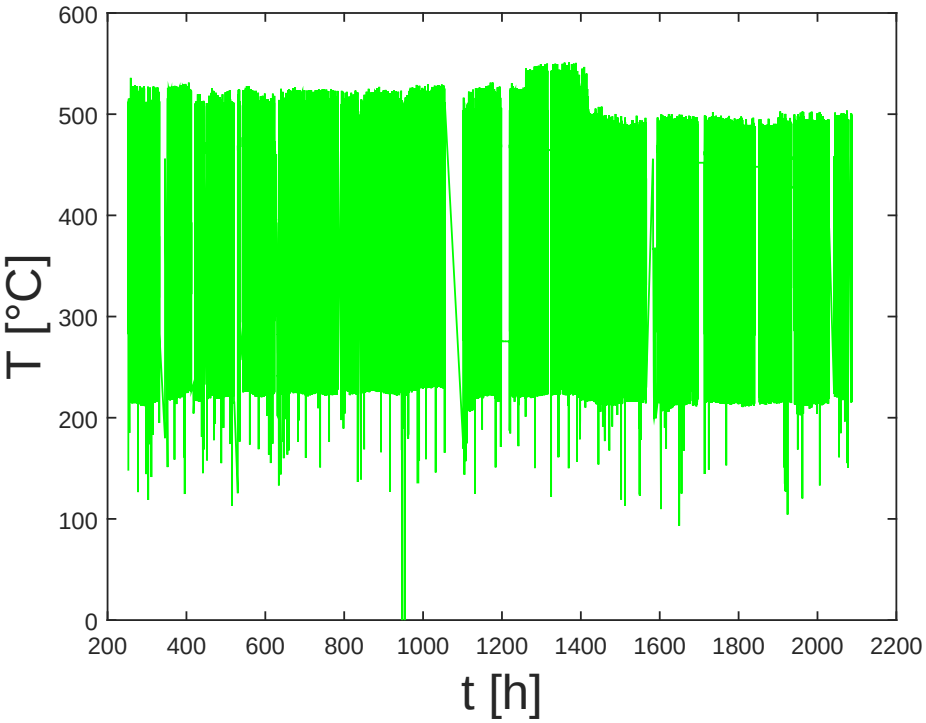

Figure B.6: Whole test bench engine temperature profile for 68719xxx.x.

Appendix C

Temperature Histograms

The temperature loads of the whole runs were approximated with short repeated recorders with high time resolution. Histograms with a bin width of 100 °C are presented in *Figures* C.1 to C.6 in order to compare the validity of the recorder representing the whole run. The reason for choosing a wider bin in this section than in the model is that the time resolution in the whole run is very poor and hence a more narrow bin would not be better. Subfigures with notation *a* have been obtained from *Figures* B.1 to B.6 and subfigures with notation *b* have been obtained from *Figures* 2.1 to 2.6. The histograms for the whole runs were calculated with all available data. The histograms for the recorders were calculated with looping the short recorders until the last activity measurement.

As there is a different time resolution and a variable step length in the whole run, there is no trivial way of comparing the two. The whole runs' histograms were approximated according to:

$$bin_i = bin_i + (t_j - t_{j-1}), \qquad \forall\,(t_j - t_{j-1}) < 0.25\,\mathrm{h} \tag{C.1}$$

The condition is needed for the missing fragments in the whole runs. Due to thermal inertia there is a overestimation of lower temperatures, which is clear for most runs when comparing to the recorder.

C.1 Model Cycles

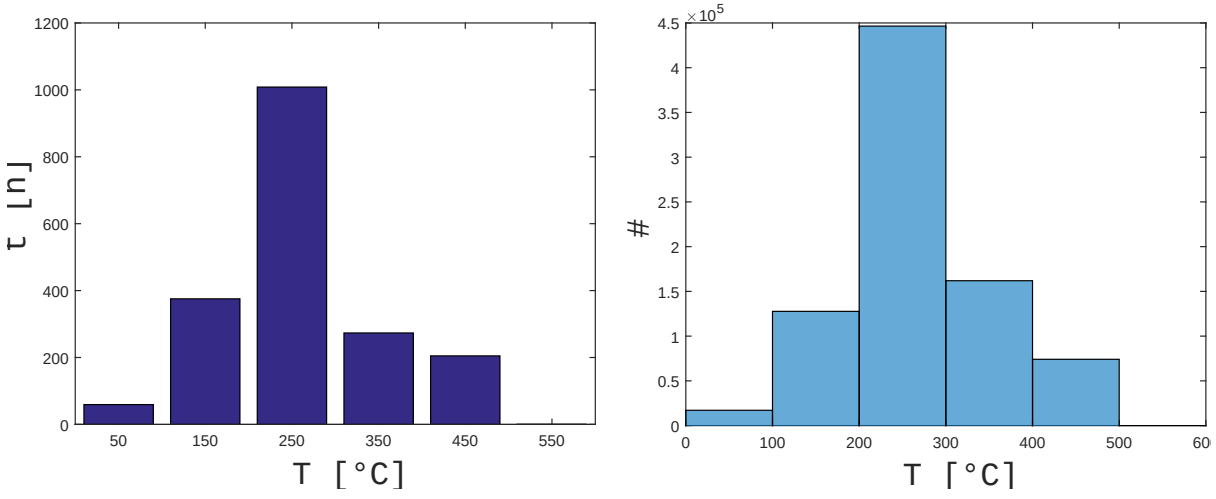

(a) Whole run

(b) Recorder

Figure C.1: Temperature histograms for 68784xxx.x.

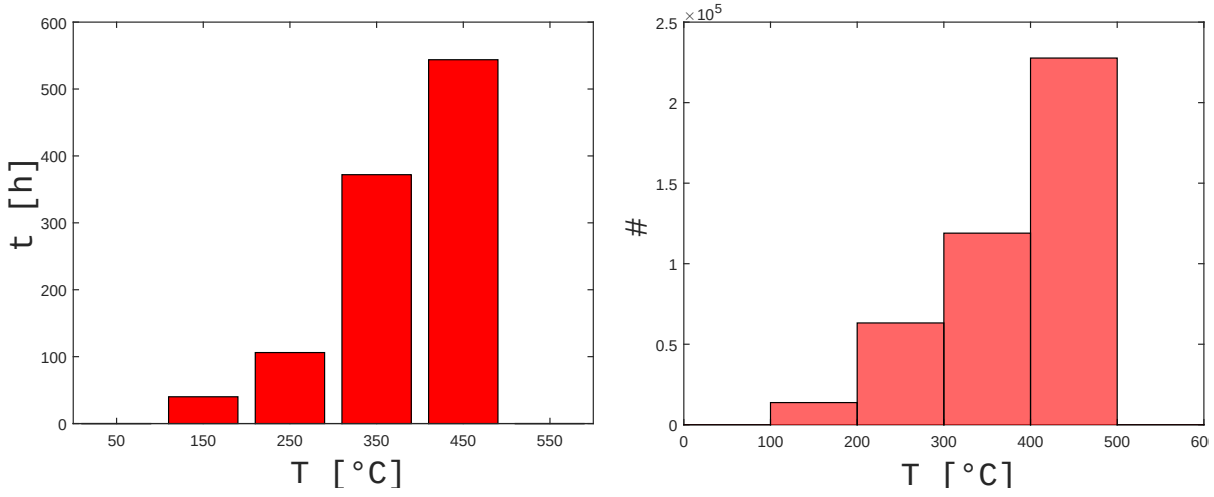

(a) Whole run (b) Recorder

Figure C.2: Temperature histograms for 68783xxx.x.

C.2 Validation Cycles

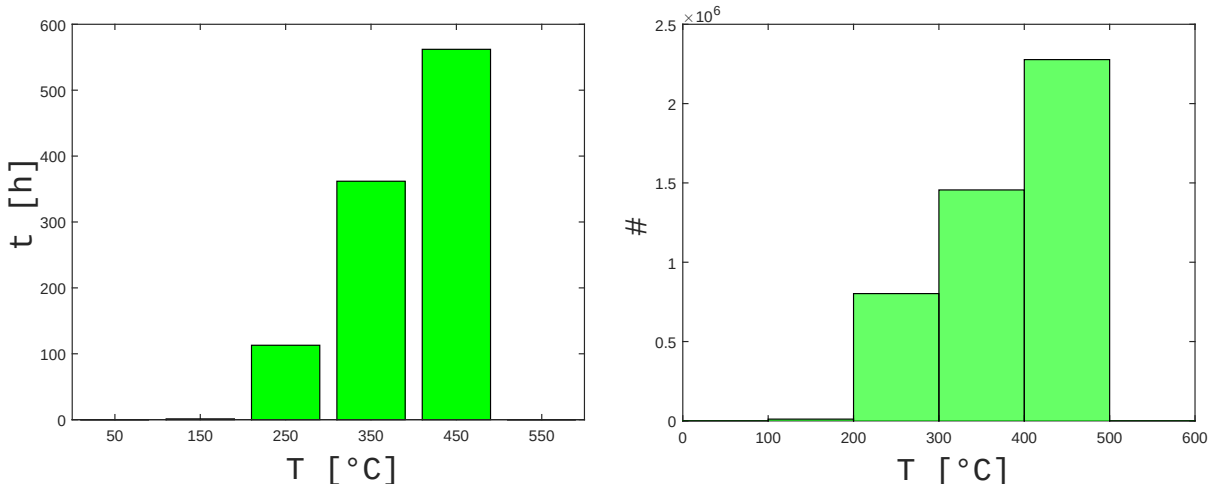

(a) Whole run (b) Recorder

Figure C.3: Temperature histograms for 68777xxx.x.

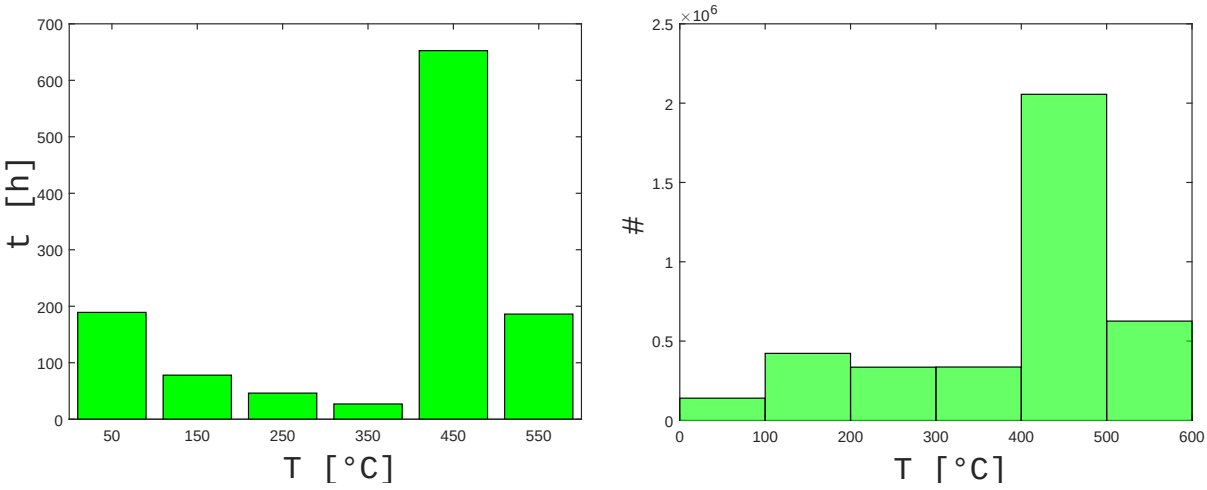

(a) Whole run (b) Recorder

Figure C.4: Temperature histograms for 68755xxx.x.

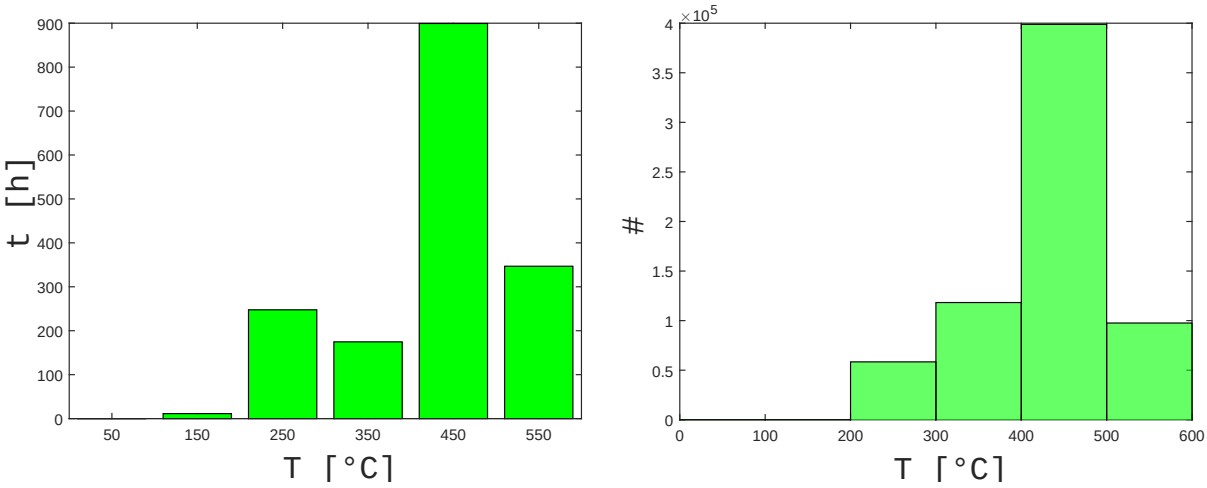

(a) Whole run (b) Recorder

Figure C.5: Temperature histograms for 68720xxx.x.

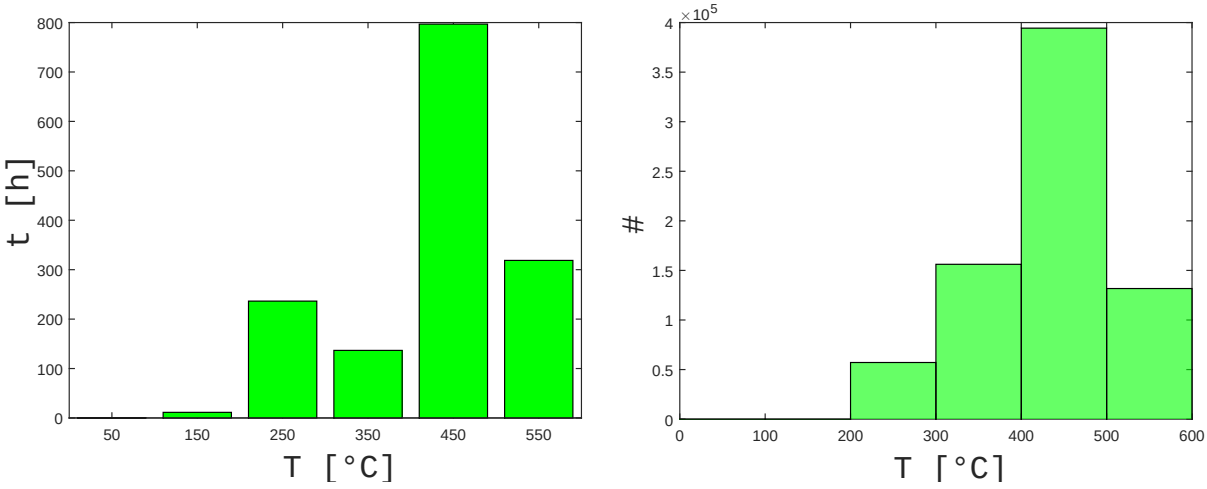

(a) Whole run (b) Recorder

Figure C.6: Temperature histograms for 68719xxx.x.

Appendix D

Variation of Assumption for Sulfur Content in Oil and Fuel

The results when varying the sulfur content in oil and fuel are presented here (*Figures* D.1 and D.2).

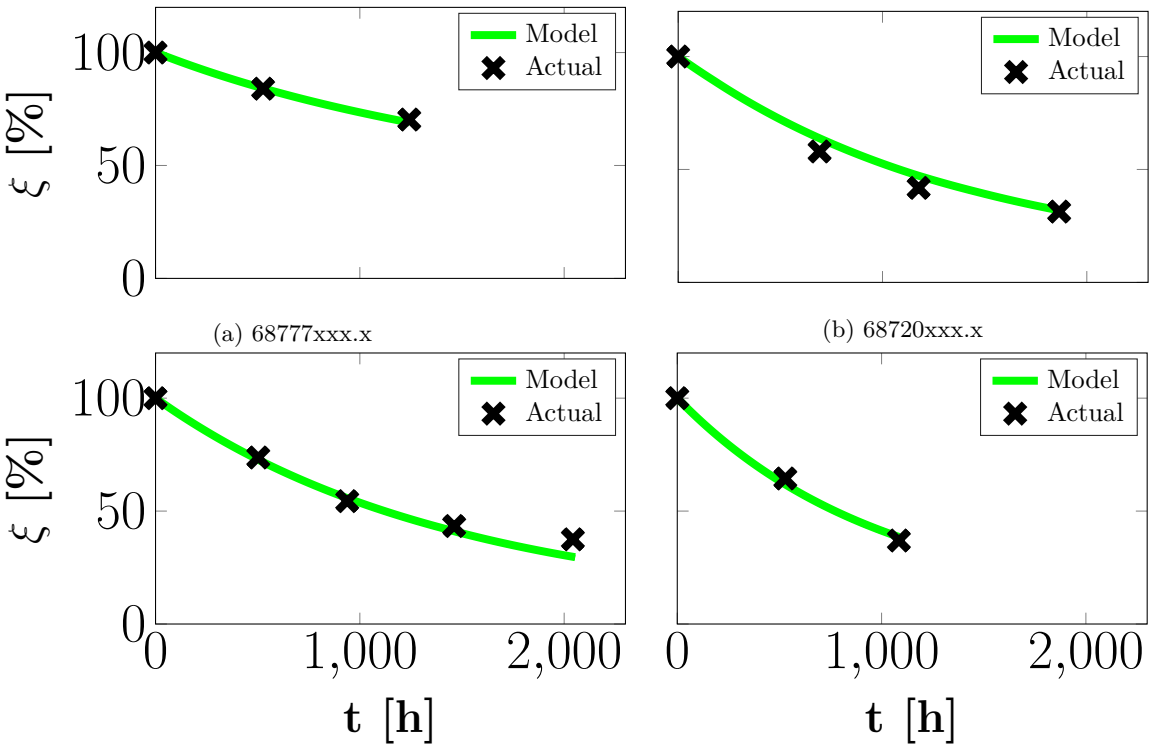

(a) 68777xxx.x

(b) 68720xxx.x

(c) 68719xxx.x

(d) 68755xxx.x

Figure D.1: Variation of sulfur content in oil where dashed and dotted line represent 2250 ppm and 3750 ppm, respectively. Subcaption refers to Concerto™ protocol.

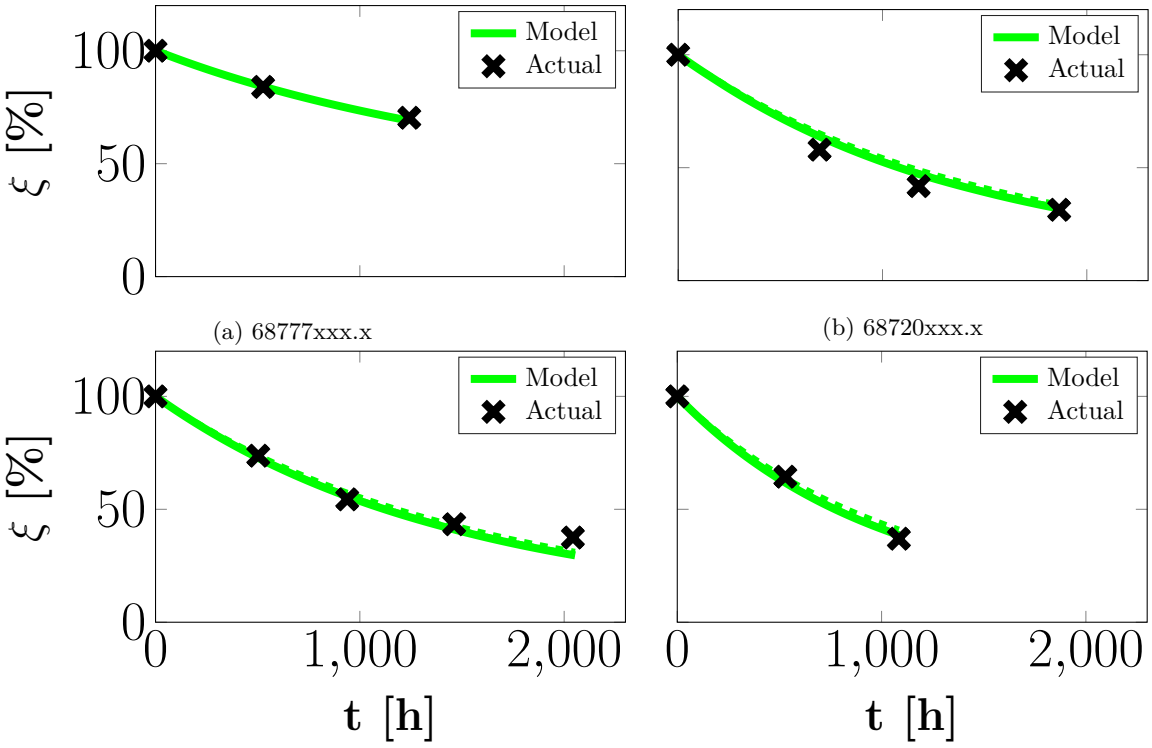

(a) 68777xxx.x

(b) 68720xxx.x

(c) 68719xxx.x

(d) 68755xxx.x

Figure D.2: Variation of sulfur content in fuel where dashed and dotted line represent 0 ppm and 10 ppm, respectively. Subcaption refers to Concerto™ protocol.